

This discussion paper is/has been under review for the journal Atmospheric Chemistry and Physics (ACP). Please refer to the corresponding final paper in ACP if available.

# Sensitivity of aerosol retrieval to geometrical configuration of ground-based sun/sky-radiometer observations

B. Torres<sup>1,2</sup>, O. Dubovik<sup>2</sup>, C. Toledano<sup>1</sup>, A. Berjon<sup>3</sup>, V. E. Cachorro<sup>1</sup>,  
T. Lapyonok<sup>2</sup>, and P. Goloub<sup>2</sup>

<sup>1</sup>Group of Atmospheric Optics, Valladolid University, Valladolid, Spain

<sup>2</sup>Laboratoire d'Optique Amosphérique, UMR8518, Université des Sciences et Technologies de Lille, Villeneuve d'Ascq, France

<sup>3</sup>Izana Atmospheric Research Center, Spanish Meteorological Agency, Tenerife, Spain

Received: 13 February 2013 – Accepted: 17 February 2013 – Published: 14 March 2013

Correspondence to: B. Torres (benjamin@goa.uva.es)

Published by Copernicus Publications on behalf of the European Geosciences Union.

ACPD

13, 6851–6921, 2013

Sensitivity of aerosol retrieval to geometrical configuration

B. Torres et al.

Title Page

Abstract

Introduction

Conclusions

References

Tables

Figures

◀

▶

Back

Close

Full Screen / Esc

Printer-friendly Version

Interactive Discussion



## Abstract

A sensitivity study of the aerosol optical properties retrieval to the geometrical configuration of the ground-based sky radiometer observations is carried out through the inversion tests. Specifically, the study is focused on the principal plane and almucantar observation, since these geometries are employed in Aeronet (AErosol RObotic NET-work). The following effects has been analyzed with simulated data for both geometries: sensitivity of the retrieval to variability of the observed scattering angle range, uncertainties in the assumptions of the aerosol vertical distribution and surface reflectance, possible instrument pointing errors and the effects of the finite field of view. The synthetic observations of radiometer in the tests were calculated using a previous climatology data of retrieved aerosol over three Aeronet sites: Mongu (Zambia) for biomass burning aerosol, Goddard Space Flight Center (Maryland-USA) for urban aerosol and Solar Village (Saudi Arabia) for desert dust aerosol. The results show that almucantar retrievals, in general, are more reliable than principal plane retrievals in presence of the analyzed error sources. This fact partially can be explained by to practical advantages of almucantar geometry: the symmetry between its left and right branches that helps to eliminate some observational uncertainties and the constant value of optical mass constant during the measurements that makes almucantar observations nearly independent on vertical variability of aerosol. Nevertheless, almucantar retrievals present instabilities at high sun observations due to the reduction of the scattering angle range coverage resulting in decrease of information content.

The last part of the study is devoted to identification of possible differences between the aerosol retrieval results obtained from real Aeronet data using both geometries. In particular, we have compared Aeronet retrievals at three different key sites: Mongu (biomass burning), Beijing (urban) and Solar Village (desert dust). Overall this analysis shows robust consistency between the retrievals from simultaneous observations in principle plane and almucantar. All identified differences are within uncertainties estimated for Aeronet aerosol retrieval. The differences in the size distribution are generally

ACPD

13, 6851–6921, 2013

## Sensitivity of aerosol retrieval to geometrical configuration

B. Torres et al.

[Title Page](#)

[Abstract](#)

[Introduction](#)

[Conclusions](#)

[References](#)

[Tables](#)

[Figures](#)

◀

▶

◀

▶

[Back](#)

[Close](#)

[Full Screen / Esc](#)

[Printer-friendly Version](#)

[Interactive Discussion](#)



under 10 % for radii between 0.1 µm and 5 µm and outside this size range, the differences can be as large as 50 %. For the absorption parameters, i.e. single scattering albedo and imaginary part of refractive index, the differences are typically under 0.01 and 0.002 respectively. The real part of the refractive index showed an error of 0.01 for biomass burning and urban aerosol and around 0.03 for desert dust.

5

## 1 Introduction

In the past decades, the study and knowledge of the atmospheric aerosol has demonstrated to have a great relevance, not only for its importance as atmospheric constituent, but also for its impact in many different aspects of the life on Earth (Solomon et al. (2007), IPCC, 2007). Indeed, aside from its importance as a pollutant (generated by industrialization and fossil fuel combustion), that has direct impact on ecosystems and human health, it has also been recognized for its influence on the global climate system. This effect is denoted as “aerosol radiative forcing” and includes the so-called direct effects, basically scattering and absorption of solar radiation, as well as indirect effects, by the modification of cloud properties (cloud lifetime, cloud albedo, precipitation, chemistry, etc.).

The aerosol particles can be natural (sea salt, desert dust, volcanic ash) or anthropogenic (nitrates, sulfates, organics, carbonaceous, etc.), or a mixture of both, with particle sizes ranging from few nanometers to hundreds of micrometers, thus leading to a complex and heterogeneous system with different physical, chemical and optical properties (Willeke and Baron (1993); D’Almeida et al. (1991)). This complexity makes it necessary to use a multidisciplinary approach for studying aerosol, that implies integrated use of very different methods and techniques.

In this context, this paper focused on the measurement and studies of the aerosol columnar properties using radiometric observation technique. This technique is based on studying the light resulted from the interaction of the solar radiation with the physical material of the aerosol particles suspended in the atmosphere. The high spatial and

ACPD

13, 6851–6921, 2013

Sensitivity of aerosol retrieval to geometrical configuration

B. Torres et al.

[Title Page](#)

[Abstract](#)

[Introduction](#)

[Conclusions](#)

[References](#)

[Tables](#)

[Figures](#)

◀

▶

[Back](#)

[Close](#)

[Full Screen / Esc](#)

[Printer-friendly Version](#)

[Interactive Discussion](#)



**Sensitivity of aerosol retrieval to geometrical configuration**

B. Torres et al.

[Title Page](#)[Abstract](#)[Introduction](#)[Conclusions](#)[References](#)[Tables](#)[Figures](#)[◀](#)[▶](#)[Back](#)[Close](#)[Full Screen / Esc](#)[Printer-friendly Version](#)[Interactive Discussion](#)

temporal variability of the aerosol properties led to the development and establishment of measurement networks covering extend areas. Among all the monitoring systems, ground based observations are been revealed as the most accurate and simplest. The most important ground based global remote sensing networks are Aeronet (Holben et al., 1998), PFR-GAW (Wehrli, 2005) and SKYNET (Takamura and Nakajima, 2004).

These networks provide the aerosol information from two kinds of spectral measurements: spectral data of direct Sun radiation attenuation by the atmosphere and angular distribution of diffused sky radiation. The direct measurements provide information about total aerosol loading (i.e., aerosol optical depth). The observation of diffuse radiation contain essential information for retrieving the aerosol phase function and optical aerosol properties. Using this information, important aerosol microphysical parameters, such as the particle size distribution (Nakajima et al., 1983, 1996) and complex refractive index or single scattering albedo (Dubovik and King, 2000; Dubovik et al., 2006), are derived.

The present work aims at identifying whether the retrieval results depend on the geometry used in the sky radiance measurements. In particular, this work has been developed with the inversion algorithm described in Dubovik and King (2000) (also Dubovik et al. (2000, 2002, 2006)), and using data provided by Aeronet. That is why the study will be focused on the almucantar and principal plane geometries (hereafter, ALM and PPL respectively), that are (Holben et al., 1998; Kaufman et al., 2002; Olmo et al., 2008), adapted as the standard observational scenarios in operational data acquisition Aeronet network (Holben et al., 1998). The measurements for same geometries are used by Skynet (Nakajima et al., 1996).

In the almucantar configuration, Fig. 1 on the left, the sun-photometers (e.g. Cimel Electronique 318, standard in Aeronet) keep the zenith angle constant (equal to the solar zenith angle  $\theta_s$ ). The azimuth movement is done first towards the right (taking the sun as reference and until  $\varphi_a = 180^\circ$ ) and then is repeated towards the left. Assuming an homogeneous atmosphere, the measurements are taken in both right and left branches are expected to be symmetrical and the final radiance values used in the in-

## Sensitivity of aerosol retrieval to geometrical configuration

B. Torres et al.

[Title Page](#)

[Abstract](#)

[Introduction](#)

[Conclusions](#)

[References](#)

[Tables](#)

[Figures](#)

[◀](#)

[▶](#)

[Back](#)

[Close](#)

[Full Screen / Esc](#)

[Printer-friendly Version](#)

[Interactive Discussion](#)



version algorithm for the almucantar is obtained by averaging observations in right and left branches. This process allows elimination of the data contaminated by sky inhomogeneities. For example, in Aeronet network processing, the measurements exhibiting radiances differences higher than 20 % between right and left branches are eliminated (this and other criteria are described in [http://aeronet.gsfc.nasa.gov/new\\_web/Documents/AERONETcriteria\\_final1\\_excerpt.pdf](http://aeronet.gsfc.nasa.gov/new_web/Documents/AERONETcriteria_final1_excerpt.pdf))

In the principal plane geometry, Fig. 1 on the right, the azimuth angle is the one that remains constant while the zenith angle varies. Note that this geometry does not present any evident symmetry and, therefore, identifying and screening sky inhomogeneities in principal plane observations is not straightforward.

Another important aspect that distinguishes ALM and PPL geometries is the relation between the scattering angle  $\Theta$ , the solar zenith angle  $\theta_s$  and the observation angles  $\theta_a$  and  $\varphi_p$  for almucantar and principal plane respectively. For any measurement, the scattering angle can be expressed as  $\cos(\Theta) = \cos^2(\theta_s) + \sin^2(\theta_s)\cos(\varphi_a - \varphi_s)$  for the almucantar<sup>1</sup>, and  $\cos(\Theta) = \cos(\theta_p \mp \theta_s)$  for the principal plane<sup>2</sup> (Nakajima et al., 1996). As a consequence, the maximum scattering angle that can be reached in both geometries is:  $\Theta_M = 2\theta_s$  in the almucantar and  $\Theta_M = \theta_s + 90^\circ$  in the principal plane.

This fact plays an important role in the present study as the information contained in the radiance measurement critically depends on the geometry selected, specially for small values of the solar zenith angle. Specifically, the first part of this work contains the analysis of the consequences of having different range of scattering angle coverage in ALM and PPL measurements. With that purpose, in section 2 we use simulated sky radiances for different  $\theta_s$  and aerosol types which will be inverted afterwards to observe the differences in the retrievals. In the same section, we include an analysis of the effect of neglecting the vertical variability of aerosol and its effects in both geometries.

<sup>1</sup>Normally, the azimuth origin is taken in the sun position and therefore  $\varphi_s = 0$ . Note that this assumption was made in Fig. 1

<sup>2</sup>The signs: (−) in the case of  $(\varphi_p - \varphi_s = 0^\circ)$  and (+) for the case of  $(\varphi_p - \varphi_s = 180^\circ)$ .

[Title Page](#)[Abstract](#)[Introduction](#)[Conclusions](#)[References](#)[Tables](#)[Figures](#)[◀](#)[▶](#)[◀](#)[▶](#)[Back](#)[Close](#)[Full Screen / Esc](#)[Printer-friendly Version](#)[Interactive Discussion](#)

Additionaly, we study the influence of some other aspects that could affect ALM and PPL in a different way, such as an uncertainties in the surface reflectance assumption, the effect of an incorrect pointing in both geometries or the effect of considering a finite field of view. Finally, we examine if the results obtained in the simulation are supported

5 by real data. For this purpose, we analyze the differences in the retrievals obtained from near-simultaneous principal plane and almucantar measurements at three different key sites.

## 2 Analysis of simulated data

### 2.1 Methodology and data

- 10 In the first section, we analyze study the variability of the retrievals for different solar zenith angles corresponding to different range of scattering angle coverage in ALM and PPL measurements. Also, in order to assure the reliability of our studies, we have conducted self-consistency tests of the inversion code. First, we simulate radiance measurements with the forward module using the pertinent size distribution and refractive index of the different aerosol examples. Then these synthetic observations are inverted 15 using the retrieval algorithm and they are compared with the assumed aerosol properties. The test are conducted for both between PPL and ALM geometries. A scheme of this procedure is drawn in Fig. 2. The test conditions, which are the solar zenith angles (5 cases:  $\theta_s = 15^\circ, 30^\circ, 45^\circ, 60^\circ$  and  $75^\circ$ ) and the measurement geometry (almucantar or principal plane), are also included in the diagram.

20 This strategy for conducting the sensitivity studies have been adapted from previous work Dubovik et al. (2000). The principal novelty here is the testing the reliability of principal plane retrievals and its comparison with those from almucantar observations. In addition, for modeling the aerosol properties we used climatology of real aerosol retrievals from Aeronet observations (described in (Dubovik and King, 2000; Dubovik et al., 2006)), Dubovik et al. (2002)) instead of using aerosol models found in

sparse literature. In that climatology analysis, characteristics of different aerosol types observed at several Aeronet key sites are derived as a function of the aerosol optical depth. Specifically, we have taken the information from three sites: Mongu (Zambia) for biomass burning aerosol, Goddard Space Flight Center (Maryland-USA) for urban

5 aerosol and Solar Village (Saudi Arabia) for desert dust aerosol. For the three examples, two possibilities for the aerosol load have been considered: the first one around the averaged value of the aerosol optical depth (registered in the study Dubovik et al. (2002)), and the second one with more aerosol load so as to see if certain conditions affect differently as the aerosol load increases.

10 Table 1 summarizes the aerosol properties of the all the examples considered. We provide full set of parameters needed to run the forward module. The first parameter is the reference value of the aerosol optical depth from which the rest of the inputs parameters are derived (using the expressions in Dubovik et al. (2002)). The next parameters in Table 1 are used to describe the size distribution (modeled as a bimodal 15 lognormal function): particle volume concentration ( $C_{V_i}$  [ $\mu\text{m}^3/\mu\text{m}^2$ ]), volume median radius ( $r_{V_i}$  [ $\mu\text{m}$ ]) and mode width ( $\sigma_{V_i}$ ), for fine and coarse mode. The rest of the inputs are the refractive index and the sphericity parameter, which is taken as 0 for desert dust (all the particles are considered to be non-spherical) and in the rest of the cases as 100 (considering all the particles as spheres).

20 The simulated aerosol optical depth and the single scattering albedo are shown in the output part of Table 1. It should be noted out that the obtained spectral aerosol optical depth does not exactly match the input values provided as reference. This can be explained by the fact that the used aerosol parameters represent the climatological regressions. Note also, that these simulated values do not depend on the “conditions” 25 such as the measurement geometry or the solar zenith angle.

In addition to the consistency check and analysis of dependence on the solar zenith angle, the same methodology is also used to analyze the sensitivity to different error sources (see the flowchart in Fig. 2. For example, to study the influence of the pointing

<a href="#">Title Page</a>	
<a href="#">Abstract</a>	<a href="#">Introduction</a>
<a href="#">Conclusions</a>	<a href="#">References</a>
<a href="#">Tables</a>	<a href="#">Figures</a>
<a href="#"></a>	<a href="#"></a>
<a href="#">Back</a>	<a href="#">Close</a>
<a href="#">Full Screen / Esc</a>	
<a href="#">Printer-friendly Version</a>	
<a href="#">Interactive Discussion</a>	

## Sensitivity of aerosol retrieval to geometrical configuration

B. Torres et al.

[Title Page](#)

[Abstract](#)

[Introduction](#)

[Conclusions](#)

[References](#)

[Tables](#)

[Figures](#)

◀

▶

◀

▶

[Back](#)

[Close](#)

[Full Screen / Esc](#)

[Printer-friendly Version](#)

[Interactive Discussion](#)



error we simulate the radiances introducing an incorrect pointing. Then these synthetic data are inverted and, the obtained results compared with the “true”—assumed ones.

## 2.2 Dependence on the solar zenith angle

The results of the consistency tests are shown in Fig. 3 for the three aerosol types considered: biomass burning aerosol (Fig. 3a), urban aerosol (Fig. 3b) and desert dust aerosol (Fig. 3c). The study is made following the scheme presented in Fig. 2. In addition to the size distribution and the refractive index (the parameters that drive the forward simulations), the single scattering albedo is also illustrated due to its great significance. The results retrieved with the almucantar geometry are shown in the upper part, while results from simulations with the principal plane are placed at the bottom in every subfigure. In all the representations, the results obtained for the case with smallest aerosol load (e.g. desert dust:  $\tau_{a_{ref}}(1020) = 0.3$ ) are plotted with a solid line while dashed line is used for the case with the largest aerosol load (e.g. desert dust  $\tau_{a_{ref}}(1020) = 0.5$ ).

Size distributions are represented in the subfigures on the right. The true size distribution used for producing the synthetic observations is plotted in black. The size distributions produced from inversion of synthetic data are plotted in different colors, depending on the solar zenith angle used for the simulations: dark blue for 15°, light blue for 30°, green for 45°, orange for 60° and brown for 75°.

The optical parameters, single scattering albedo and the refractive index, are plotted as a function of the solar zenith angle. Different colors have been chosen, in this case, for different wavelengths, thus, blue for 440 nm, green for 670 nm, yellow for 870 nm and red for 1020 nm. The input values are not shown in order to make the interpretation of the figure easier and they can be seen in Table 1.

The most evident tendency observed in the tests is the instability of the optical parameters for small solar zenith angles in the almucantar. This tendency is present in the tests for all aerosol types. For instance, the single scattering albedo differs on average around 0.02 at  $\theta_s = 15^\circ$  from those obtained at larger solar zenith angle. This latter

**Sensitivity of aerosol retrieval to geometrical configuration**

B. Torres et al.

[Title Page](#)[Abstract](#)[Introduction](#)[Conclusions](#)[References](#)[Tables](#)[Figures](#)[◀](#)[▶](#)[◀](#)[▶](#)[Back](#)[Close](#)[Full Screen / Esc](#)[Printer-friendly Version](#)[Interactive Discussion](#)

agrees with the values given in Table 1. On the other hand, the results obtained with the principal plane geometry do not have such strong dependence on the solar zenith angle. The values are shown in Table 1.

The instability in the retrievals obtained from almucantar data can be explained by the fact that only aerosol scattering in middle and large scattering angles depends on complex index of refraction and the forward peak of aerosol phase function is dominated by light diffraction (Bohren and Huffman, 1983). In this regard, for almucantar observational geometry the maximum scattering angle is  $2\theta_s$ , i.e. the measurements corresponding to small solar zenith angles do not contain enough information to adequately retrieve the index of refraction and consequently the single scattering albedo. The same result was described for simulations in Dubovik et al. (2000), and for real Aeronet data in Dubovik (2009).

In the refractive index analysis, we observe the same result; for the principal plane, the retrievals are stable and the values correspond to those given in Table 1 (the only exception is found for the case of the biomass burning at  $\theta_s = 15^\circ$ ). On the other hand, the retrievals obtained for the almucantar drift further apart from their input values as the solar zenith angle is getting smaller. The worst behavior can be found in the case of the desert dust with low aerosol load, where the real part of refractive index is 0.1 smaller than the assumed value at  $\theta_s = 15^\circ$  (1.46 when it should be 1.56), and the imaginary part is much higher than the inputs, specially for long wavelengths where values are three times larger.

From the analysis of the differences in the size distribution a dependency on the radius can be seen: the differences observed between the retrievals and the input values do not exceed 10 % for intermediate radii (in both retrievals ALM and PPL) while they strongly increase in the extremes. In the cases of urban and desert dust, these intermediate radii are confined between  $0.1 \mu\text{m}$  and  $5 \mu\text{m}$ , while for biomass burning the interval is smaller: between  $0.3 \mu\text{m}$  and  $3 \mu\text{m}$ . Moreover, the differences between the assumed and the retrievals (and between the retrievals themselves (PPL vs ALM))

**Sensitivity of aerosol retrieval to geometrical configuration**

B. Torres et al.

[Title Page](#)[Abstract](#)[Introduction](#)[Conclusions](#)[References](#)[Tables](#)[Figures](#)[◀](#)[▶](#)[◀](#)[▶](#)[Back](#)[Close](#)[Full Screen / Esc](#)[Printer-friendly Version](#)[Interactive Discussion](#)

are much higher for the case of biomass burning, which are over 100 %, than for urban and desert dust, which are only up to 40 %.

The analysis of the differences for the biomass burning, illustrated in Fig. 3, shows noticeable differences in the fine mode only when the maximum scattering angle is smaller than  $120^\circ$  ( $\theta_s = 15^\circ, 30^\circ, 45^\circ$  for almucantar and  $\theta_s = 15^\circ$  for the principal plane simulations), and specially for the case with larger aerosol load (named as Zamb2) where the values of the size distribution get unexpectedly higher than the original size distribution (up to 20 %). This effect is accompanied by a sharp decline in the real refractive index (from 1.51 to 1.47–1.48). Both effects compensate each other for the calculation of optical thickness: there are more particles but they scatter less light. There is a strong connection between the retrieved fine mode and the real part of the refractive index and this fact will be recurrent in the next studies. Nevertheless, the disagreements are more striking in the coarse mode. For principal plane, all the size distributions are separated from the original one when the radius is higher than  $3\text{ }\mu\text{m}$ . They all have the same values and decrease faster than the input for radii above  $3\text{ }\mu\text{m}$ . For the almucantar, nonetheless, the size distributions also get away from the original but they do not have a defined direction.

The larger discrepancies in the extremes can be explained by the very low sensitivity of radiometer observations to the size distribution variation for the radius smaller than  $0.1\text{ }\mu\text{m}$  or larger than  $3\text{ }\mu\text{m}$  for the wavelengths used in Aeronet (Dubovik et al. (2000)). In particular for the case of biomass burning, this effect gets more important since its coarse mode is displaced towards larger radius ( $r_{V_c}$  for Mongu site is the largest among the selected examples) while for the other examples the volume concentration in this size region is quite lower. Finally, we conclude that the tests did not reveal any systematic pattern of differences between the retrievals obtained through PPL and ALM. The larger noise in the extreme compare to the one for the central radii is the only effect observed.

## 2.3 Dependence on the aerosol vertical distribution

Once analyzed the discrepancies obtained due to the different scattering angle coverage of both geometries, the next step is the study of the influence of some other aspects that could affect ALM and PPL differently. First we analyze the effect of the aerosol vertical distribution variability in the atmosphere. As mentioned in the introduction and illustrated in Fig. 1, the zenith angle is kept constant during measurement in the almucantar and the observation in the almucantar has a symmetry whereas principal plane does not.

The second, and a less obvious, characteristic of observations in the almucantar is its low dependence on the aerosol vertical variability that, is generally, weaker than that for observations in principle plane. This can be illustrated with the following brief analysis of solution of radiative transfer equation in single-scattering approximations for almucantar and principle plane geometries.

Let us consider the solution of the radiance  $R$  for the first-order scattering and for any observation angle  $\theta_v$  given by,

$$R = \frac{F_0}{|\mu_v|} e^{-\tau/\mu_v} \times \int_0^{z_t} \left( \sum_k M_k \right) e^{-m' t(z)} dz \quad (1)$$

where

$$\tau = \int_0^{z_t} \sum_k \sigma_{\text{ext}_k}(z) dz \quad (2)$$

20

$$t(z) = \int_0^z \sum_k \sigma_{\text{ext}_k}(z') dz' \quad (3)$$

[Title Page](#)[Abstract](#)[Introduction](#)[Conclusions](#)[References](#)[Tables](#)[Figures](#)[◀](#)[▶](#)[◀](#)[▶](#)[Back](#)[Close](#)[Full Screen / Esc](#)[Printer-friendly Version](#)[Interactive Discussion](#)

$$M_k = \frac{\omega_{o_k} P_k \sigma_{\text{ext}_k}(z)}{4\pi} \quad (4)$$

5  $m' = \frac{1}{\mu_s} - \frac{1}{|\mu_v|}$ ; with  $(5)$

$$\mu_s = 1/\cos \theta_s \text{ and } \mu_v = 1/\cos \theta_v \quad (6)$$

10 Observe that we have included k-components at any height  $z$  of the atmosphere. The parameters  $P_k$  and  $\sigma_{\text{ext}_k}$  are respectively the phase function and the extinction coefficient for every single component. However, in the almucantar observations  $\mu_s = \mu_v$  and Eq. (1) should be rewritten as,

$$R_a = \frac{F_0}{\mu_s} e^{-\tau/\mu_s} \times \int_0^{z_t} \left( \sum_k M_k \right) dz \quad (7)$$

15 The phase function,  $P_k$ , and the single scattering albedo,  $\omega_{o_k}(z)$ , for every single component do not depend on the height and can be taken out of the integral.

$$R_a = \frac{F_0}{\mu_s} e^{-\tau/\mu_s} \times \left( \sum_k \omega_{o_k} \tau_k P_k \right) \quad (8)$$

where

$$\tau_k = \int_0^{z_t} \sigma_{\text{ext}_k}(z) \quad (9)$$

## Sensitivity of aerosol retrieval to geometrical configuration

B. Torres et al.

[Title Page](#)

[Abstract](#)

[Introduction](#)

[Conclusions](#)

[References](#)

[Tables](#)

[Figures](#)

◀

▶

◀

▶

[Back](#)

[Close](#)

[Full Screen / Esc](#)

[Printer-friendly Version](#)

[Interactive Discussion](#)



Eq. (8) is already independent from the height. Therefore, for the single scattering approximation in the almucantar geometry, the radiance measurements do not depend on the vertical distribution of the components in the atmosphere, and particularly, on the aerosol vertical distribution.

- 5 Note, that typically, we consider three main components: gaseous absorption, molecular scattering (Rayleigh), and aerosol scattering and absorption and Eq. (8) is rewritten as:

$$R_a = \frac{F_0}{\mu_s} e^{-\tau/\mu_s} [\omega_o \tau_a P_a + \tau_R P_R] \quad (10)$$

with

$$10 \tau = \tau_{\text{abs}}^{\text{gas}} + \tau_{\text{scat}}^a + \tau_{\text{abs}}^a + \tau_R \quad (11)$$

The exponential term within the integral in the general equation, Eq. (1), links the principal plane measurement to the aerosol and gas vertical distribution. Only in the case that we consider just one main layer in the atmosphere (without any changes in the vertical distribution), we could deduce a similar expression for the principal plane as in Eq. (10),

$$15 R_p = \frac{F_0 \mu_s}{\mu_v - \mu_s} \left[ \frac{\omega_o \tau_a P_a + \tau_R P_R}{\tau_a + \tau_R} \right] [e^{-\frac{\tau}{\mu_v}} - e^{-\frac{\tau}{\mu_s}}] \quad (12)$$

Consequently, in the single scattering approximation, a heterogeneous aerosol vertical distribution would only affect to the principal plane. Multiple scattering effects of the light in the atmosphere add some sensitivity to vertical variability of atmosphere for both observations in almucantar and principal plane. Nonetheless, since the transmitted radiation of aerosol is dominated by the effects of the first order of scattering the dependence of radiances in almucantar to vertical variability of the atmosphere is generally weaker than for radiances measured in principal plane.

[Title Page](#)[Abstract](#)[Introduction](#)[Conclusions](#)[References](#)[Tables](#)[Figures](#)[◀](#)[▶](#)[◀](#)[▶](#)[Back](#)[Close](#)[Full Screen / Esc](#)[Printer-friendly Version](#)[Interactive Discussion](#)

**Sensitivity of aerosol retrieval to geometrical configuration**

B. Torres et al.

[Title Page](#)[Abstract](#)[Introduction](#)[Conclusions](#)[References](#)[Tables](#)[Figures](#)[◀](#)[▶](#)[Back](#)[Close](#)[Full Screen / Esc](#)[Printer-friendly Version](#)[Interactive Discussion](#)

The above conclusion suggests, that some differences between aerosol retrievals from simultaneous measurements in principle plane and almucantar can appear due to their different sensitivity to the assumptions regarding aerosol vertical distribution. This aspect is of particular interest for present study, because generally there is no reliable information for making accurate assumption about aerosol vertical distribution. Only in situations when co-located data from the lidar are available the accounting for detailed aerosol vertical distribution is possible (e.g. Lopatin et al., 2013).

To analyze the effects of the vertical distribution, we produced the synthetic observations using the aerosol properties of urban (GSFC2) and desert dust (Solv2). The forward calculations were conducted using the assumption of multi-layers plane parallel atmosphere: 30 equidistant in pressure layers were used. Utilizing the same idea as in Sinyuk et al. (2007), we used two different aerosol vertical distributions: two Gaussian profiles with 1 km width and median height of aerosol concentration profile at ground level and at 3 km respectively (Sinyuk et al. (2007), Fig. 1.). To check the possible dependency of the results on  $\theta_s$ , we have done the tests for  $\theta_s = 45^\circ$  and  $\theta_s = 75^\circ$ . First, the simulated radiances for both geometries were inverted under the assumption of mono-layered. This assumption is used in operational Aeronet (Dubovik and King, 2000) and Sky-Net processing (Nakajima et al., 1996).

Figure 4 represents the size distributions retrieved under the previously mentioned conditions for urban (left) and desert dust (right) aerosol types. Note that in total, there are eight size distributions for each aerosol case corresponding to every possible combination between the two geometries, the two vertical aerosol profiles and the two solar zenith angles.

The results obtained are quite similar for both aerosol types. For almucantar geometry, the size distributions retrieved do not display any significant differences compared to the assumed “true” values. Only small differences can be observed in the coarse mode for desert dust at  $\theta_s = 75^\circ$ , where the effect of multiple scattering is more important. The maximum of these differences is observed for  $r = 3 \mu\text{m}$  with a value around 10 %. In contrast, principal plane results show two interesting tendencies: on the one

## Sensitivity of aerosol retrieval to geometrical configuration

B. Torres et al.

[Title Page](#)

[Abstract](#)

[Introduction](#)

[Conclusions](#)

[References](#)

[Tables](#)

[Figures](#)

◀

▶

◀  
Back

▶  
Close

[Full Screen / Esc](#)

[Printer-friendly Version](#)

[Interactive Discussion](#)



hand the results for  $\theta_s = 45^\circ$  do not significantly differ from the input size distributions for both aerosol types; while, on the other hand, they present important differences in the case of  $\theta_s = 75^\circ$ , specially for the fine mode, where they reach values over 50 %.

This interesting result confirms the theoretical expectations foreseen above: the principal plane retrieval are more likely affected by aerosol vertical distribution than almucantar inversion. The simulations reveal the larger differences with the assumed values for the geometries with large solar zenith angles, especially for the size distribution in the fine mode. The retrieval errors appear to be larger when the aerosol concentration profile median height is assumed at ground than when it is at 3 km.

The addition of extra layers in the retrieval process is particularly simple in those cases where the aerosol vertical distribution is known, as well as the distributions of other atmospheric components. Figure 5 provides the results when additional layers are added during the inversion process for the particular case of urban aerosol at  $\theta_s = 75^\circ$  with principal plane measurements. Subfigure in the right represents the case with the aerosol distribution profile with the maximum concentration at ground level, and subfigure in the left represents the case with the maximum at 3 km. Red and blue lines denote the retrievals for 2-layers and 5-layers respectively, defining the border between layers equidistant in pressure.

If the vertical structure of the aerosol is known, the accurate aerosol profile can be used in the retrieval. In such conditions, all retrieved properties can adequately retrieved from both geometries. Figure 5 shows the results for the retrieval using accurate vertical profile for the case of urban aerosol at  $\theta_s = 75^\circ$  measured in principal plane. Subfigure in the right represents the case with aerosol concentration profile median height at ground level, and subfigure in the left represents the case with the maximum at 3 km. Red and blue lines denote the retrievals for 2-layers and 5-layers respectively, defining the border between layers equidistant in pressure.

However, in practice the accurate information about vertical distribution of the aerosol is rarely available, while vertical profile may change quite dramatically. Therefore, in this study we are interested to find out if taking into account of, at least, some general

# Sensitivity of aerosol retrieval to geometrical configuration

B. Torres et al.

features characteristic for vertical distribution of the atmosphere may reveal any advantages compare with using the base assumption of mono-layered atmosphere. With that purpose, first we have investigated the effect of straightforward reduction of vertical resolution of multi-layered atmosphere (assuming correct aerosol profile in the inversion).

- 5 The assumption of bi-layered atmosphere substantially improves the results compare  
to mono-layered atmosphere retrievals (shown in Fig. 4), specially for the case when  
the aerosol concentration profile median height is at 3-km where the errors are practi-  
cally negligible. In the case when the aerosol median height is at the ground level, the  
errors are around 20 %, but they are diminishing as the number of assumed layers is  
increased. For instance, if the retrieval is provided with 5-layers the errors are under  
10 5 % for both cases.

Nevertheless, the above tests were done using the known vertical profile of aerosol, that generally is not known. Therefore, in the second series of tests, we have focused on the evaluation of the possibility to use generic assumption of bi-layered atmosphere

- 15 where the lower layer contains aerosol mixed with Rayleigh scattering while the upper layer contains only Rayleigh scattering. Indeed, in the real atmosphere molecular scattering generally dominates at the altitudes above  $\sim 5$  km. In Fig. 5, gray lines represent these alternative solutions: solid line when the border between the layers is fixed at 2 km, dash line when the border is at 4 km and dash-dotted when is at 6 km.

Using the second assumption leads to generally worse results compare to retrievals obtained using accurate aerosol vertical distribution. Furthermore, there is no an optimum choice of the altitude to put the border between the two layers. Thus, in the first representation, i.e. the case with the maximum aerosol concentrations at ground level, the border assumption providing the best results was the one located at 2 km

- 25 and the size distributions retrieved deteriorated with the increase of the border altitude. On the other hand, the case with the maximum aerosol concentrations at 3 km showed the opposite tendency and the results improved with increase of the border of layer altitude.

Title Page

## Abstract

Introduction

## Conclusions

## References

Tables

Figures



Back

Close

Full Screen / Esc

[Printer-friendly Version](#)

## Interactive Discussion



**Sensitivity of aerosol retrieval to geometrical configuration**

B. Torres et al.

[Title Page](#)[Abstract](#)[Introduction](#)[Conclusions](#)[References](#)[Tables](#)[Figures](#)[◀](#)[▶](#)[Back](#)[Close](#)[Full Screen / Esc](#)[Printer-friendly Version](#)[Interactive Discussion](#)

**Sensitivity of aerosol retrieval to geometrical configuration**

B. Torres et al.

[Title Page](#)[Abstract](#)[Introduction](#)[Conclusions](#)[References](#)[Tables](#)[Figures](#)[◀](#)[▶](#)[Back](#)[Close](#)[Full Screen / Esc](#)[Printer-friendly Version](#)[Interactive Discussion](#)

For the cases without extra information about the aerosol vertical profile, the strategy of the two layers described here provides the same results as for the size distribution. In this particular case, when the border is situated at 2 km there are almost no differences and as the border is getting higher the differences appear. Nevertheless, the proposed intermediate solution of settling the border at 4 km still presents acceptable differences around 0.01 in the real part of the refractive index.

Thus, overall the tests showed that for inversions of the radiances measured in almucantar the vertical variability of aerosol is not an issue, and assumption of mono-layered atmosphere does not results in any notable retrieval errors. This conclusion can also be extended for the aerosol retrieval from principle plane with a unique exception of the observations at the large solar zenith angles. At the same time, for the last scenario, the retrieval errors can be practically eliminated by assuming generic bi-layered: aerosol+Rayleigh/Rayleigh atmosphere. These conclusions support the retrieval settings adapted for operational for operational retrieval in Aeronet network: the aerosol vertical distribution is assumed homogeneous in the almucantar inversion and bi-layered for the principal plane inversion. ([http://aeronet.gsfc.nasa.gov/new\\_web/Documents/Inversion\\_products\\_V2.pdf](http://aeronet.gsfc.nasa.gov/new_web/Documents/Inversion_products_V2.pdf)).

## 2.4 Dependence on the surface reflectance

The second aspect under discussion will be dependence on the surface reflectance for both geometries. With this purpose, we will introduce an aleatory error in the surface reflectance during the inversion procedure, in order to study the effects on the retrievals. In its current version, the inversion algorithm (described in Dubovik and King, 2000) approximates the surface reflectance by a Bi-directional Reflectance Function (BDRF). Cox-Munk model is used for retrievals over water (Cox and Munk, 1954) and Lie-Ross model over land (Lucht and Roujean, 2000). This surface description is also currently used in Aeronet retrievals ([http://aeronet.gsfc.nasa.gov/new\\_web/Documents/Inversion\\_products\\_V2.pdf](http://aeronet.gsfc.nasa.gov/new_web/Documents/Inversion_products_V2.pdf)). The BDRF parameters are basically three:  $\rho_o(\lambda)$ ,  $\kappa(\lambda)$  and  $\Theta(\lambda)$  which characterize the intensity of reflectance, the anisotropy of reflectance and

**Sensitivity of aerosol retrieval to geometrical configuration**

B. Torres et al.

[Title Page](#)[Abstract](#)[Introduction](#)[Conclusions](#)[References](#)[Tables](#)[Figures](#)[◀](#)[▶](#)[Back](#)[Close](#)[Full Screen / Esc](#)[Printer-friendly Version](#)[Interactive Discussion](#)

the forward/backscattering contribution in the total reflectance, respectively, and they are adopted from MODIS Ecotype generic BRDF models.

The following scheme is used for the tests: first radiances are simulated (as in Fig. 2) with the typical BDRF parameters observed in the three sites (see Table 3). Then, 5 the data are inverted for 200 different scenarios using BDRF parameters perturbed by gaussian noise. Specifically, the errors in  $\rho_o$  will be relative errors generated randomly from a normal distribution with mean 0 and standard deviation 15 %, with a limit up to  $\pm 30\%$ . The errors in  $\kappa(\lambda)$  and  $\Theta(\lambda)$  will be absolute errors generated randomly, and with values of the standard deviations of 0.05 and 0.025 respectively; the error limits 10 will be established as  $\pm 0.1$  for  $\kappa(\lambda)$  (with  $\kappa(\lambda) > 0$ ) and 0.05 for  $\Theta(\lambda)$ .

In the illustrations of the results, we focus on the analysis of the cases (from Table 1) with the largest aerosol load for the three aerosol types; as in the previous section, we will only evaluate the cases at  $\theta_s = 45^\circ$  and  $\theta_s = 75^\circ$ .

Figures 6 and 7 depict the means and the standard deviations of the differences 15 between the 200 retrievals and the non-error case. The results are shown for principal plane and almucantar geometry and for each aerosol type: biomass burning (Zamb2, at the top), urban (GSFC2, in the middle) and desert dust (SolV2, at the bottom). Relative differences have been used for the analyses of the size distribution (figures in the left), while the differences in the optical parameters are provided in absolute terms.

Analyzing the outcomes, there are two results that stand out from the rest. First, as 20 we have considered random errors, there is no a clearly defined tendency in the mean of the differences. In the size distribution, for instance, the means rarely exceed 10 % and their sign do not follow a clear pattern. In the optical parameters the means are also very small; in this way, the maximum mean of the absolute difference for the single scattering albedo is 0.003. Therefore, the analysis needs to be done in terms of the standard deviation which contains, in this case, the information about the dependency 25 on the surface reflectance error of the retrieved products. Secondly, and from this new approach, it can be seen that the error in the surface reflectance affects more at  $\theta_s = 45^\circ$  than at  $\theta_s = 75^\circ$ . The last result is even more notorious for the principal plane

**Sensitivity of aerosol retrieval to geometrical configuration**

B. Torres et al.

[Title Page](#)[Abstract](#)[Introduction](#)[Conclusions](#)[References](#)[Tables](#)[Figures](#)[◀](#)[▶](#)[◀](#)[▶](#)[Back](#)[Close](#)[Full Screen / Esc](#)[Printer-friendly Version](#)[Interactive Discussion](#)

geometry as it will be commented. For instance, if we start the study with the size distribution, while in the almucantar we observe a small improvement of the results from  $\theta_s = 45^\circ$  to  $\theta_s = 75^\circ$ , the improvement in the principal plane is considerably more notorious.

- 5 The analysis of the results leaded to two main conclusion. First, the introduction of the random errors in the surface reflectance assumption did not results to any retrieval bias. For example, in the size distribution differences the means rarely exceed 10 % and their signs do not follow a clear pattern. For the optical parameters the means are also very small and the maximum mean of the absolute difference for the single scattering 10 albedo is 0.003. Second, both the bias and, specially the standard deviations (plotted as error bar) from the analysis on the surface reflectance are more pronounced at  $\theta_s = 45^\circ$  than at  $\theta_s = 75^\circ$ .

The highest values of the means and the standard deviations are observed for the fine mode for desert dust and urban aerosols at  $\theta_s = 45^\circ$ , as commented. For both 15 cases, all the standard deviations for radii smaller than 0.3  $\mu\text{m}$  are over 10 %, reaching the maximum of 22 % at 0.02  $\mu\text{m}$  in the desert dust. For larger radii, both the means and the standard deviations of the differences are reduced, the latter rarely exceeds 5 % when the radii are larger than 0.3  $\mu\text{m}$ ; the only exception is the relative large values observed for the principal plane when radii are larger than 5  $\mu\text{m}$ . On the other hand, 20 the results for biomass burning do not depend on the radii. In this case, the maximum values of the means are around 8 % and the standard deviation about 12 %.

As mentioned above, the retrieval results are more accurate at  $\theta_s = 75^\circ$ . The means 25 of the differences are smaller than 5 % in the urban and in the biomass burning. For the desert dust, there are some values of the principal plane retrievals in the fine mode and some values of the almucantar retrievals in the coarse mode which are larger than the 5 %. In fact, the results for the almucantar retrieval of the coarse mode are worse than at  $\theta_s = 45^\circ$ .

In the single scattering albedo the means of the differences are smaller than 0.003 for all the simulations. The standard deviations are similar for the three aerosol cases

[Title Page](#)[Abstract](#)[Introduction](#)[Conclusions](#)[References](#)[Tables](#)[Figures](#)[◀](#)[▶](#)[◀](#)[▶](#)[Back](#)[Close](#)[Full Screen / Esc](#)[Printer-friendly Version](#)[Interactive Discussion](#)

being the maximum values around 0.013, reached at  $\theta_s = 45^\circ$ . It can be also observed, that the principal plane values are slightly higher than the almucantar ones. Following the general outcome, the results are better at  $\theta_s = 75^\circ$  with maximum of the standard deviations 0.008. The improvement is more notorious in the principal plane resulting in lower values of the standard deviations than almucantar at this solar zenith angle.

Similar result is found for the refractive index: at  $\theta_s = 45^\circ$ , the results for almucantar retrieval are better, while at  $\theta_s = 75^\circ$  they are not as good as the principal plane ones. For the real part, the maximum of the standard deviation is around 0.03 at  $\theta_s = 45^\circ$  (reached in principal plane geometry) and around 0.02 (reached in almucantar geometry).

For the imaginary part, the biomass burning case shows larger standard deviations than the other two cases, due to its larger absorption. The maxima at  $\theta_s = 45^\circ$  and at  $\theta_s = 75^\circ$  are reached for this aerosol type, with values 0.0028 and 0.0015 respectively. For urban and desert dust, the standard deviations are smaller than 0.001 for both solar zenith angles.

In summary, the observed differences in the optical parameters are relatively small considering the magnitude of the errors that we have introduced in the surface reflectance assumption. Nevertheless, the effects of surface reflectance uncertainties are slightly higher for the size distribution specially in the fine mode.

## 20 2.5 Dependence on the pointing error

The pointing error is defined as the angle between the Sun position (correct pointing) and the erroneous pointing direction. As sun-photometers are moved by two motors, azimuth and zenith axes, the value of the pointing error,  $\Theta_\xi$ , is normally given in spherical coordinates:

$$25 \quad \Theta_\xi = \Theta_\xi(\xi_\varphi, \xi_\theta) \quad (13)$$

where  $\xi_\varphi$  and  $\xi_\theta$  are the error components in azimuth and zenith angles respectively. Considering the pointing error sufficiently small, it can be expressed as an infinitesi-

## Sensitivity of aerosol retrieval to geometrical configuration

B. Torres et al.

[Title Page](#)

[Abstract](#)

[Introduction](#)

[Conclusions](#)

[References](#)

[Tables](#)

[Figures](#)

◀

▶

[Back](#)

[Close](#)

[Full Screen / Esc](#)

[Printer-friendly Version](#)

[Interactive Discussion](#)

mal displacement in spherical coordinates (with  $dr = 0$ ) and therefore the relation in Eq. (13) takes the following form:

$$\Theta_\xi = \xi_\theta \hat{\theta} + \sin \theta_s \xi_\varphi \hat{\varphi} = \sqrt{\xi_\theta^2 + \sin \theta_s^2 \xi_\varphi^2} \quad (14)$$

The work by Torres (2012) describes a methodology used for the characterization of these magnitudes and a first evaluation of the results for several individual instruments (all of them Cimel 318 sun-photometers). One of the main outcomes of this evaluation is that the magnitudes  $\xi_\theta$  and  $\sin \theta_s \xi_\varphi$  are constant for each photometers regardless  $\theta_s$ . This result indicates that the pointing error,  $\Theta_\xi$ , can be understood as the scattering angle between the Sun beam and the direction where the detector (in charge of the sun pointing process in the instrument) is pointing and that is constant through the day. In the present work, the characteristics magnitudes  $\Theta_{\xi_\theta} = \xi_\theta$  and  $\Theta_{\xi_\varphi} = \sin \theta_s \xi_\varphi$ , will be named as total vertical and horizontal error, respectively, keeping the names of zenith and azimuth error for  $\xi_\theta$  and  $\xi_\varphi$ .

The first tests, done with 8 photometers in the work by Torres (2012), showed that for most of the instruments the magnitudes of  $\xi_\theta$  and  $\sin \theta_s \xi_\varphi$  were smaller than  $0.1^\circ$ . The maximum values obtained for vertical and horizontal error were  $0.25^\circ$ , while the maximum of total error  $\Theta_\xi$  was  $0.35^\circ$ . In this section we will use for the simulations a pointing error value of  $0.4^\circ$  (horizontal and vertical) as it is the maximum realistic error that can be committed without affecting the aerosol optical depth and therefore not noticeable in the data obtained from Aeronet network (the value of the field of view is around  $1.2^\circ$  in the standard sun-photometers of the network).

The scheme for this study is similar to the one presented in Fig. 2, but introducing the pointing errors in the forward code. As commented, the value of the simulated pointing error is  $0.4^\circ$  and considering positive or negative errors for vertical component and only positive errors for the horizontal component. The vertical error can be committed from the Sun towards the zenith or towards the Earth surface, which results in different consequences in almucantar and principal plane measurements, and therefore, both possibilities should be considered. In this study, the sign of the error is established as

## Sensitivity of aerosol retrieval to geometrical configuration

B. Torres et al.

[Title Page](#)

[Abstract](#)

[Introduction](#)

[Conclusions](#)

[References](#)

[Tables](#)

[Figures](#)

◀

▶

◀

▶

[Back](#)

[Close](#)

[Full Screen / Esc](#)

[Printer-friendly Version](#)

[Interactive Discussion](#)



positive in the case of variation towards the zenith, and negative in the case of variation towards the Earth surface.

As for the horizontal error, it can be committed either to the left or to the right of the Sun. In the principal plane, regardless of the error direction, the consequences are symmetric. In the almucantar, the errors are initially not symmetric but due to the possibility of averaging the left and the right branches, they become symmetric. As a consequence, for both geometries, there is no need to consider the sign of the horizontal error and only the absolute value is relevant. Note also that the averaging process produces that in the almucantar the horizontal error effect is much weaker than in the principal plane.

The results for the simulations of the pointing error test are presented in Fig. 8 for the size distribution, in Fig. 9 for the single scattering albedo and in Fig. 10 for the refractive index. In each figure, the results are depicted for the three aerosol types considered: biomass burning aerosol (a), urban aerosol (b) and desert dust aerosol (c). For each aerosol type, results retrieved with the almucantar geometry are shown in the upper part, while results from simulations with the principal plane are placed at the bottom. The subfigures on the left correspond to retrievals with vertical errors (positive and negative), and the ones on the right to horizontal errors (only positive). Note that the X-axis is the radius for the size distribution and different colors represent different solar zenith angle; for the optical parameters the X-axis is precisely the solar zenith angle and the colors distinguish between the wavelengths.

Analyzing the Fig. 8, the first thing we observe is that there are only remarkable differences respect to the results obtained in Fig. 3 for the cases involving principal plane and vertical errors, i.e. there are no differences in the almucantar regardless the error pointing type, neither in the principal plane with horizontal error.

Centering the study on the case with vertical errors in PPL, the aerosol type showing the largest differences is desert dust, where for the case with a positive vertical error there is a 10 % decrease in the size distributions between 1  $\mu\text{m}$  and 3  $\mu\text{m}$  and a little increment around 4–5 % for larger radii. With negative vertical error, the situation is

## Sensitivity of aerosol retrieval to geometrical configuration

B. Torres et al.

[Title Page](#)

<a href="#">Abstract</a>	<a href="#">Introduction</a>
--------------------------	------------------------------

<a href="#">Conclusions</a>	<a href="#">References</a>
-----------------------------	----------------------------

<a href="#">Tables</a>	<a href="#">Figures</a>
------------------------	-------------------------

◀

▶

◀

▶

[Back](#)

[Close](#)

[Full Screen / Esc](#)

[Printer-friendly Version](#)

[Interactive Discussion](#)



the opposite: there is a big increase up to 15–20 % for radii between 1  $\mu\text{m}$  and 3  $\mu\text{m}$  accompanied by a significant reduction for larger radii.

In the other two aerosol cases, and specially for urban aerosol, we can see the behavior of the fine mode which is opposite to that of the coarse mode: it grows for positive errors and decreases for negative errors. To be more precise, the perturbations are only observed for radii smaller than 0.3  $\mu\text{m}$ , and in general, they are smaller than the ones found in the coarse mode. Moreover, the differences, between the results found here and the ones obtained in section 2.2, depend on  $\theta_s$  and on the aerosol load being larger as both parameters are smaller. The values of these differences are normally under 20 %. However, the maximum values are around 50 % and they are found for the urban case at  $\theta_s = 15^\circ$  with the lowest aerosol load and at radii between 0.05 and 0.2  $\mu\text{m}$ .

To explain these results, we necessarily need to check the differences in the radiance measurements that the pointing errors generate. For this purpose, radiance relative differences are represented in Fig. 11, for vertical errors in almucantar and principal plane in the upper part, and for horizontal errors in the subfigures at the bottom. We have only taken the differences for GSFC aerosol not to be repetitive as there are no relevant differences respect to the other aerosol types. Note also that the differences are plot against the scattering angle and at different  $\theta_s$  (from left to the right at 15°, 45° and 75°).

The relative differences generated by vertical errors in the principal plane (see Fig. 11) are 5 times larger than the ones originated in the almucantar and a magnitude order larger than the differences generated by horizontal errors in both geometries. This fact explains why the largest differences found in Fig. 8 are for vertical errors in principal plane geometry. We observe, as well, that the results for positive and negative vertical errors are symmetric in the principal plane (not in the almucantar). These differences are positive for small scattering angles when the errors are negative, and they are negative for positive errors. At large scattering angles the relation is the opposite: positive for positive errors and negative for negative errors.

## Sensitivity of aerosol retrieval to geometrical configuration

B. Torres et al.

[Title Page](#)

[Abstract](#)

[Introduction](#)

[Conclusions](#)

[References](#)

[Tables](#)

[Figures](#)

[◀](#)

[▶](#)

[◀](#)

[▶](#)

[Back](#)

[Close](#)

[Full Screen / Esc](#)

[Printer-friendly Version](#)

[Interactive Discussion](#)



## Sensitivity of aerosol retrieval to geometrical configuration

B. Torres et al.

[Title Page](#)

[Abstract](#)

[Introduction](#)

[Conclusions](#)

[References](#)

[Tables](#)

[Figures](#)

◀

▶

◀

▶

[Back](#)

[Close](#)

[Full Screen / Esc](#)

[Printer-friendly Version](#)

[Interactive Discussion](#)



with less aerosol load in the three examples; in the same manner the differences are smaller as the aerosol is more absorbing. Maximum differences of 0.02 are found for desert dust while the minimum differences are reached in the biomass burning, which are smaller than 0.01.

- 5 The presence of positive vertical error in the principal plane geometry diminishes the radiance at small scattering angles while at the rest there is no variation. For negative errors we observe the opposite result. Due to this fact, real part of refractive index is expected to enlarge (or to shrink for negative) to a great extent. And this is exactly what it is found in the desert dust example where the real part raises from 1.56 to the highest
- 10 value (1.6) allowed by the inversion process in all the channels. For the negative error, it falls to values between 1.49 and 1.52 varying for the channel and for the  $\theta_s$ .

However, for the other two aerosol types, the real part of the refractive index decreases for a positive error, which is in disagreement with the previous argument. It should be remembered that this idea was used successfully in the desert dust case  
 15 and as the radiance differences in all the cases present the same behavior, apparently there is no immediate explanation for the different behavior. A possible explanation could be obtained analyzing the size distributions: In the desert dust case for positive vertical errors, the retrievals from principal planes gave a decrease of the coarse mode and no variations in the fine mode. More light for longer scattering angle with less particles could be only explained with a strong increase in the real refractive index. But for urban and biomass burning examples, the fine mode increases for vertical pointing errors. In this second scenario, if the increment of the particles is very strong, even in the case of more light, the real refractive index can drop, even more, if we consider the strong connection between real part of refractive index and fine mode of the size distribution, commented in previous sections.  
 20

There are two ideas supporting this argument. First, the variation of the real part is minor for the 1020 nm channel but it becomes greater as the wavelength is shorter, or on other words, is larger at wavelengths more affected by the fine mode. Needless to say, that for negative errors the explanation above is valid but changing the sign  
 25

## Sensitivity of aerosol retrieval to geometrical configuration

B. Torres et al.

[Title Page](#)

[Abstract](#)

[Introduction](#)

[Conclusions](#)

[References](#)

[Tables](#)

[Figures](#)

[◀](#)

[▶](#)

[◀](#)

[▶](#)

[Back](#)

[Close](#)

[Full Screen / Esc](#)

[Printer-friendly Version](#)

[Interactive Discussion](#)



of the variations. The second proof is that the real part is more stable for the biomass burning example (more absorbing than urban), for the largest aerosol optical depth and for the largest solar zenith angles, which were the same conditions that we found for the smallest variations in the size distributions.

If we analyze now the effect of vertical errors on almucantar measurements, we observe that the radiance relative differences (in Fig. 11), are positive for  $\theta_s = 15^\circ$ , negative for  $\theta_s = 75^\circ$  and close to zero at  $\theta_s = 45^\circ$  when the pointing error is positive. As a consequence,  $\omega_o$  will increase at small scattering angles and decrease at large scattering angles. This tendency is found in the three aerosol types presented. Note, that this drift is opposite to the fictitious  $\omega_o$  cycle presented in Sect. 2.2 for almucantars.

When vertical errors are negative, there are negative differences for  $\theta_s = 15^\circ$  and positive differences for  $\theta_s = 75^\circ$ , finding no differences again at  $\theta_s = 45^\circ$ . Thus,  $\omega_o$  would have the opposite behavior: reduction for small  $\theta_s$  and increment for large  $\theta_s$ . Therefore, negative vertical pointing errors will enlarge the fictitious daily cycle of  $\omega_o$  in almucantar retrievals. Both results are confirmed in Fig. 9.

The imaginary part of the refractive index responds in the same way as the single scattering albedo, but its variations have the opposite sign. Again, both parameters are less affected for the case of biomass burning as its absorption is greater than in the other two cases. The real part does not suffer relevant variations at the presence of vertical error in the almucantar geometry.

Finally, we want to indicate that the optical parameters analyzed do not suffer any variations respect to reference cases presented in Fig. 3 for horizontal errors in both geometries.

## 2.6 Dependence on the finite field of view

The concept of sky radiance can be defined as the radiant flux per unit projected area and per unit solid angle coming from a specified point in the sky (McCluney, 1994). That is why, ideally, the observational solid angle should be infinitesimal. However, the

**Sensitivity of aerosol retrieval to geometrical configuration**

B. Torres et al.

[Title Page](#)[Abstract](#)[Introduction](#)[Conclusions](#)[References](#)[Tables](#)[Figures](#)[◀](#)[▶](#)[Back](#)[Close](#)[Full Screen / Esc](#)[Printer-friendly Version](#)[Interactive Discussion](#)

inversion algorithms, which use radiance measurements as input, assume this approximation considering the instrument field of view as punctual.

Nevertheless, the instruments have a finite field of view, specially in the case of the sun-photometer CIMEL-318, the value of the field of view is  $1.2^\circ$  in the actual instruments and in old versions  $2.4^\circ$ .

The effect of the finite field of view on the radiance measurement in every observation point is obtained by the convolution of the viewing geometry and the angular values of the sky radiance. In Torres (2012), several test done with the sun-photometer CIMEL-318 showed that the response of its field of view can be approximated as a cylinder.

Using this result, the convolution is simplified as a surface integral of the radiance function within the field of view region. In our approach, the integral is substituted by a discrete sum considering 17 points in the field of view range around the observation point, see Fig. 12. As the areas are chosen in order to be equal, the fore-mentioned surface integral is approximated by averaging the sky radiance values obtained in the 17 selected points.

The test are done considering values of the field of view of  $1.2^\circ$  or  $2.4^\circ$  in every measurement point for the almucantar and for the principal plane geometries. As in previous analysis, the study is done using the 3 aerosol examples described and at 5 solar zenith angles ( $15^\circ$ ,  $30^\circ$ ,  $45^\circ$ ,  $60^\circ$  and  $75^\circ$ ).

The results obtained simulating a field of view of  $1.2^\circ$  (non plotted) are the same that the ones obtained in Fig. 3. It can be concluded, therefore, that the actual field of view of  $1.2^\circ$  do not include any variations respect to the non-error case.

On the other hand, the results for a field of view of  $2.4^\circ$  indicate that the variations respect to the non error data set are only relevant for the real part of the refractive index. Specifically, in the almucantar, the results obtained for  $\theta_s = 15^\circ$  are around 3 % lower than in Fig. 3, for the rest of the solar zenith angles the differences are negligible. For the principal plane, the real part show smaller oscillations, under 3 %, but they appear for all the solar zenith angles.

### 3 Check of the simulations against real data

In order to complete the work, we propose a parallel study with real data comparing the retrievals of principal plane and almucantar. With this aim, data from three Aeronet sites characteristic of three different types of aerosol are chosen: Mongu (Zambia, 15.25° S–23.15° E, 1107.0 m.s.l.) is chosen for the analysis of biomass burning aerosol, Beijing (China, 39.98° N–116.38° E, 92.0 m.s.l.) for urban aerosol and Solar Village (Saudi Arabia, 24.90° N–46.40° E, 790 m.s.l.) for desert dust aerosol. We only select data which accomplished the next four requirements: (1) Data with aerosol optical depth belonging to Aeronet Level 2.0 (not asked for retrievals, because we are interested also in almucantar data with  $\theta_s < 50^\circ$ ); (2) Data from those days where the ratio between the standard deviation and the average of the aerosol optical depth values is smaller than 0.1 (evaluated for the four wavelengths used by the inversion 440, 670, 870 and 1020 nm). This requirement is established in order to assure that the analysis is done for stable aerosol conditions. (3) The pairs almucantar and principal plane are selected only if both measurements took place within a maximum delay of 30 minutes. 4. Finally, only those days presenting at least 4 pairs matching the previous three conditions are chosen for the comparison.

Following these previous requirements, a total of 207 pairs have been taken for the comparison, of which 65 pairs belong to biomass burning (top-left in Table 4), 59 pairs to urban aerosol (top-right in Table 4) and 83 pairs to desert dust. The latter set was divided, in two subgroups as it will be commented later (Table 4 at the bottom, left and right).

The comparison for Mongu includes data from 2003 to 2009 for 4 different sunphotometers. It is worth mentioning that we have guaranteed that the data correspond to biomass burning events by the application of typical thresholds for Angstrom exponent values in biomass burning (Eck et al., 1999). As a consequence, all the days found are contained in the period from July to October. Mongu is mainly sandy with a

<a href="#">Title Page</a>	
<a href="#">Abstract</a>	<a href="#">Introduction</a>
<a href="#">Conclusions</a>	<a href="#">References</a>
<a href="#">Tables</a>	<a href="#">Figures</a>
<a href="#">◀</a>	<a href="#">▶</a>
<a href="#">◀</a>	<a href="#">▶</a>
<a href="#">Back</a>	<a href="#">Close</a>
<a href="#">Full Screen / Esc</a>	
<a href="#">Printer-friendly Version</a>	
<a href="#">Interactive Discussion</a>	

**Sensitivity of aerosol retrieval to geometrical configuration**

B. Torres et al.

[Title Page](#)[Abstract](#)[Introduction](#)[Conclusions](#)[References](#)[Tables](#)[Figures](#)[◀](#)[▶](#)[◀](#)[▶](#)[Back](#)[Close](#)[Full Screen / Esc](#)[Printer-friendly Version](#)[Interactive Discussion](#)

seasonal flood plain that is burned to the west annually from July through November (see Mongu site description in Aeronet website).

The comparison in Beijing can be seen on the top right part of Table 4. All the data selected belong to autumn and winter. We have selected data corresponding to urban/industrial aerosol with similar features as those described by Dubovik et al. (2002) (predomination of the fine mode with Angstrom exponent values higher than 1.7). In spring, there are frequently desert dust events while in summer the elevated relative humidity and temperature result in great hygroscopic aerosol growth increasing the coarse mode concentration (Eck et al., 2005).

Eventually, the data corresponding to the comparison in Solar Village, used in order to do the analysis of desert dust aerosol, are contained at the bottom part of Table 4. The reason for splitting those data in two groups was taken during the evaluation of the comparisons ALM-PPL. At this point, we observed that for some photometers (Table 4 bottom part on the left) the results presented a similar aspect to the ones obtained for the two previous aerosol types, whereas for some other photometers the comparison achieved was much worse (Table 4, bottom part on the right), especially in the size distribution as it will be shown in the next section. Nevertheless, this case presents a higher number of days with stable conditions providing enough data to carry out the double analysis.

### 3.1 Size Distribution

Figure 13 represents the mean and standard deviation (error bars) of the relative differences obtained for the comparison of the size distribution in the three analyzed cases: biomass burning (upper part of the figure, data from the top-left part of Table 4) urban (central part of the figure, data from the top-right part of Table 4) and desert dust (lower part of the figure, only the data from the bottom-left of Table 4).

Observing the figure, we can see how the comparisons for the three aerosol types present similar results as those obtained in the self-consistency analysis from the previous section: There is a general good agreement for radii between 0.1  $\mu\text{m}$  and 5  $\mu\text{m}$ ,

with values of the average of the relative differences under 10 %, except for the radii around 2  $\mu\text{m}$  where the average is a bit higher, reaching maximum values up to 20 %. Thus, these differences are a bit higher than those obtained over simulated data. At this point, we should remember the possibility of having errors, e.g. the ones we have studied in the previous analysis, could provoke the increase. Nevertheless, the errors are still within the interval 15% – 25 % which is the expected accuracy suggested by Aeronet for almucantar retrievals.

Moving to the extremes, for radii smaller than 0.1  $\mu\text{m}$  or larger than 5  $\mu\text{m}$ , the comparison is much worse than in the previous analyzed region as it was expected. The relative differences are much larger, up to 60 %, but still similar to those obtained in the previous section and within the confident interval given by Aeronet for these radii (up to 100 %). The unexpected result is that these differences are positive, indicating that the values in the size distribution obtained from the almucantar are systematically lower than those obtained using the principal plane.

Among the three aerosol types, the biomass burning shows the smallest discrepancies in the extremes; for this aerosol type, the differences are under 22 % except for the last bin (at 15  $\mu\text{m}$ ) where the relative difference is 44 %. Desert dust case presents the worst behavior, specially in the coarse mode, where for several bins the relative differences exceed 40 % reaching the maximum of 60 % at 11.4  $\mu\text{m}$ .

## 3.2 Optical parameters

Table 5 contains the mean values and the standard deviations obtained for the single scattering albedo and the refractive index in the analyzed days using only almucantar geometry. The values obtained for the biomass burning aerosol in Mongu and for the desert dust in Solar Village are similar to those presented in Table 1. For instance,  $\omega(440) = 0.85$  corresponding to the analysis of the biomass burning is comparable to the one obtained  $\omega(440) = 0.88$ .

Finally, it should be noted that Beijing site was not included neither in the previous section nor in the analysis done in Dubovik et al. (2002); however, the mean values

**Sensitivity of aerosol retrieval to geometrical configuration**

B. Torres et al.

[Title Page](#)[Abstract](#)[Introduction](#)[Conclusions](#)[References](#)[Tables](#)[Figures](#)[◀](#)[▶](#)[◀](#)[▶](#)[Back](#)[Close](#)[Full Screen / Esc](#)[Printer-friendly Version](#)[Interactive Discussion](#)

found for the urban aerosol of this analysis agree with the typical values of the several urban aerosol examples presented in Dubovik et al. (2002).

Returning to the comparison between the principal plane and almucantar retrievals, the results for the single scattering albedo are shown in Fig. 14. The mean of the differences between both inversions are plotted against the wavelength for the three aerosol cases analyzed: biomass burning (gray), urban (blue) and desert dust (orange). The standard deviation of the differences is represented using the error bar. As it can be seen in the plot, the average of the differences is under 0.01 for the three analyzed cases and for the four wavelengths, reaching the highest value (0.007) at 440 nm for the desert dust. On the other hand, the standard deviation is under 0.01 for the biomass burning and the urban aerosol, being a bit higher for the desert dust aerosol where values around 0.02 are obtained. Nevertheless, this result is due to the effect of the problem regarding the almucantar angle coverage: if we reduce the analyses to those cases with  $\theta_s < 50^\circ$ , the standard deviation reduces it values considerably, specially for the desert dust where  $\sigma = 0.01$ . It should be commented that the uncertainty given by Aeronet for  $\omega_o$  is 0.03 which highlights the extraordinary agreement obtained here.

Figure 15 shows the results for the real part of the refractive index. The averaged values of the difference for biomass burning and urban aerosol are lower than 0.005 indicating that there is no tendency between principal plane and almucantar differences; on the contrary, the average for the desert dust is about 0.03, or in other words, the values of the real part of the refractive index retrieved using principal plane are on average significantly higher than the ones obtained using almucantar for the desert dust. The standard deviation does not depend on the aerosol type, with a value about 0.03 for the three cases. These results are not improved when limiting the study to  $\theta_s < 50^\circ$ . Nonetheless, the accuracy given for this parameter is 0.03 for biomass burning and urban and a bit higher, 0.05, for desert dust; therefore the results are within this interval.

Eventually, Fig. 16 depicts the averages and the standard deviations of the absolute differences for the imaginary part of the refractive index. Contrary to the previous cases, the highest standard deviations of the absolute differences are reached for the biomass

burning aerosol presenting values around 0.003. On the other hand, the values for desert dust and urban aerosol are enclosed between 0.0014 and 0.002. It should be remembered (Table 5), that the absolute values of the imaginary part of the relative index for the biomass burning are one order of magnitude higher than those for the desert dust and around twice as large as the ones for the urban aerosol. Therefore, in relative terms, the best comparison is obtained again for biomass burning and urban aerosol. The strong correlation between the imaginary part of the refractive index and the single scattering albedo makes that the mean values of the two magnitudes present their sign exchanged for the three cases and the four wavelengths. Using Table 5, we observe that the average of the differences, principal plane vs almucantar, of the imaginary part of the refractive index are at maximum 8 % for the desert dust aerosol, 6 % for the urban aerosol and 4 % for biomass burning. We should note again that the expected accuracy is 30 % for strongly absorbing aerosol and 50 % for weakly absorbing aerosol, values notably improved in the comparison here.

### 15 3.3 Desert dust II: data sub-set with larger discrepancies

As it was just shown, the comparisons obtained from desert dust aerosol have larger error than for the other aerosol types. Moreover, for some photometers these differences were substantially larger. This was the case of photometers #233 and #33 (called Desert dust II); the results obtained for these photometers were systematically worse for every single pair of data compared. However, these discrepancies can not be attributed to the differences in the aerosol measured, since the intrinsic characteristics (both optical and physical parameters) are similar to the ones found for the previously analyzed cases; as an example, for each mode of the volume particle size distribution [ $dV(r)/d\ln r$ ] mean values of the particle volume concentration, the median radius, and the standard deviation (obtained only using almucantar inversions) are represented for both desert dust sets in Table 6. The values observed are very similar for both groups showing that the higher discrepancies obtained for Desert dust II pairs can not be justified by differences in the shape of the size distribution. Note here as well, that the

[Title Page](#)[Abstract](#)[Introduction](#)[Conclusions](#)[References](#)[Tables](#)[Figures](#)[◀](#)[▶](#)[◀](#)[▶](#)[Back](#)[Close](#)[Full Screen / Esc](#)[Printer-friendly Version](#)[Interactive Discussion](#)

**Sensitivity of aerosol retrieval to geometrical configuration**

B. Torres et al.

values of the median radius and the standard deviation for the coarse mode ( $r_{Vc}$  and  $\sigma_{Vc}$ ) shown in Table 1 were 2.32 and 0.6 which are in a perfect agreement with the ones obtained in the two subgroups here.

The upper chart in Fig. 17 contains the average of the relative differences and the standard deviation obtained from the comparison between the retrievals using principal plane and almucantar in the sub-set Desert dust II. The most outstanding result is the strong increase of the values in the extremes ( $r < 0.1 \mu\text{m}$  and  $r > 5 \mu\text{m}$ ) compared to the previous analyzed cases. For the coarse mode, the values of the average are over 100 %. However, the averaged values for the central are similar to the previous cases being under 20 %. We find an exception for the radii between  $3 \mu\text{m}$  and  $5 \mu\text{m}$ , where the differences, affected by the strong increase in the extremes, present values up to 60 %. In the same way, the standard deviation shows a similar behavior, doubling its value in the extremes (from 30 %–40 % it increases to 60 %) but keeping around 20 % in the central part.

The central and the bottom chart of Fig. 17 correspond to the same analysis (photometers #233 and #33) but limiting the study to those cases where the solar zenith angle is larger than  $30^\circ$  and  $50^\circ$  respectively. As it can be seen, both limitations improve the comparison considerably. The comparison for solar zenith angles larger than  $30^\circ$  eliminates 11 pairs of data (from 33 to 22) and the results, especially the average value of the relative differences are diminished reaching similar values as the ones obtained for the photometers classed in the sub-set Desert Dust I. Again, another 11 pairs of data disappear when the limitation is extended until  $50^\circ$ ; under this criterion, the average values do not suffer any improvements but the standard deviations are appreciably lower specially for  $r > 3 \mu\text{m}$ .

Continuing with the analysis of the data set Desert dust II, the results for the optical parameters are depicted in Table 7. Averaged values and the standard deviations of the differences between the retrievals of principal plane and almucantar are presented for all data (upper part of the Table 7), those data with  $\theta_s > 30^\circ$  (central part of the Table 7) and only for those cases where  $\theta_s > 50^\circ$  (bottom part of the Table 7).

[Title Page](#)[Abstract](#)[Introduction](#)[Conclusions](#)[References](#)[Tables](#)[Figures](#)[◀](#)[▶](#)[◀](#)[▶](#)[Back](#)[Close](#)[Full Screen / Esc](#)[Printer-friendly Version](#)[Interactive Discussion](#)

The means of the differences observed for the whole data set are, in general, considerably larger than the values observed in the data set Desert dust I (Figs. 14–16). Thus, averaged differences are around three times larger for the single scattering albedo and for the imaginary part of the refractive index in this data set than those obtained for the  
5 Desert dust I. In the same manner, the values of the standard deviation are typically twice as large.

On the other hand, the real part of the refractive index presents similar means of the differences than those obtained for the data set Desert dust I. Nevertheless, the values of the standard deviation for this parameter are again twice as large as the ones shown  
10 in Fig. 15.

Finally, it should be indicated that the differences descend, for the three parameters analyzed, once we limit the study to those data with  $\theta_s > 30^\circ$  and  $\theta_s > 50^\circ$ . The values of the differences for both restricted data set (presented in the central and bottom part of Table 7) are similar to the ones obtained in the study for Desert dust I.

## 15 4 Discussion

No comprehensive analysis of the advantages and disadvantages of almucantar with respect to principal plane can be found in the literature. Nevertheless, among aerosol community there is generally higher confidence in the almucantar retrievals. Indeed,  
20 most of the works presented in the literature where aerosol microphysical properties are retrieved using sun and sky radiance measurements have been done exclusively using almucantar measurements (Holben et al., 2001; Smirnov et al., 2002; Dubovik et al., 2002; Eck et al., 2010; Giles et al., 2011, to cite some), with few exceptions in which principal plane geometry is used (Vermeulen et al., 2000; Olmo et al., 2008; Valenzuela et al., 2012a,b).

25 Moreover, only retrievals obtained from the almucantar are provided by Aeronet, even though the inversion strategy does not reveal any clear preference in the geometry of the radiance measurement. Nonetheless, the success of the network resides in

[Title Page](#)[Abstract](#)[Introduction](#)[Conclusions](#)[References](#)[Tables](#)[Figures](#)[◀](#)[▶](#)[Back](#)[Close](#)[Full Screen / Esc](#)[Printer-friendly Version](#)[Interactive Discussion](#)

## Sensitivity of aerosol retrieval to geometrical configuration

B. Torres et al.

[Title Page](#)

[Abstract](#)

[Introduction](#)

[Conclusions](#)

[References](#)

[Tables](#)

[Figures](#)

◀

▶

[Back](#)

[Close](#)

[Full Screen / Esc](#)

[Printer-friendly Version](#)

[Interactive Discussion](#)



the reliability of its products, and the fore-mentioned larger confidence granted by the almucantar. The question is whether this decision is fully justified or not.

The main reason for limiting the aerosol retrieval to almucantar geometry is the great advantage provided by the symmetry existing in the almucantar measurements. First it helps to reduce the error effects by taking the average of left and right branches, resulting in more stable measurements. Additionally the symmetry allows to perform a cloud screening which cannot be so easily implemented for the principal plane. Both the sensitivity tests with the introduced modeled errors and the analysis of real data confirmed the greater reliability assumed for almucantar retrievals. It was shown here that the average between the left and right branches in the almucantar largely diminishes the consequences of possible pointing offsets in the instruments, while for the principal plane the consequences of such errors are more significant. Furthermore, almucantar retrievals have shown less dependency on the aerosol vertical distribution, as generally expected from theoretical considerations.

On the other hand, one of the main results of the conducted sensitivity studies and real data analysis is the larger stability of principal plane retrievals throughout the day, compared to the retrievals obtained from almucantar data. Indeed, the retrievals from almuncatars taken at high solar elevation show significant drop in accuracy for most of the retrieved aerosol parameters, while the principle plane retrievals remain stable in the course of the day (Fig. 3). This result was already well discussed in Dubovik et al. (2000) and is accounted for the quality selection criteria (summarized in Dubovik et al. (2002)) and adapted for Level 2 retrieval in Aeronet version 2, where only retrievals with  $\theta_s > 50^\circ$  are accepted. One of the immediate consequences of the selection of the almucantar geometry is the lack of high accuracy aerosol retrievals during the middle of the day (except at high latitudes), which is highly desirable for the various aerosol studies. Therefore, the elimination of the principle plane data generally leads to significant reductions in the amount of the data available for users.

Even though the reliability of the data is one of the primary objectives of the Aeronet network, the complete elimination of principle plane retrievals from the provided aerosol

## Sensitivity of aerosol retrieval to geometrical configuration

B. Torres et al.

## 5 Conclusions

The simulated studies carried out in this work have overall showed that, in an ideal situation with no extra errors introduced, the observations from the principal plane geometry provide more reliable results than those from almucantar due to lower information content in the almucantar radiances for high Sun observation where the range of observed scattering angles is substantially reduced.

However, the symmetry existing for the almucantar geometry confers a greater robustness of the aerosol retrievals in presence of various systematic uncertainties. For example, the straightforward symmetry check is used in aerosol quality screening to eliminate sky inhomogeneities. Also, the present study has showed that if the pointing errors are present, the consequences on principal plane retrievals are much larger than for almucantar retrievals.

The comparison between the retrievals of principal plane and almucantar obtained  
with real data has shown that the differences in the products are, in general, within  
Aeronet estimated uncertainties for almucantar retrievals.

6887



The differences between the retrievals of the size distribution are generally under 10 % for radii between 0.1  $\mu\text{m}$  and 5  $\mu\text{m}$ . Outside this size range, the differences can be as large as 50 % and mostly positive (i.e. principal plane inversion results in larger concentration than the almucantar). This result was expected due to the loss of sensitivity of the retrievals to particles of those sizes for the wavelengths used in Aeronet and it was previously obtained with simulated data (similar result also in Dubovik et al. (2000)).

The low sensitivity in the extremes provokes as well that the values in the extreme radii of the size distribution have a small interaction with the other aerosol properties retrieved, such as the aerosol optical depth or the optical parameters. Actually, even though there are differences over 50 % in the bins in the extreme of the size distribution, differences in the optical parameters are almost negligible (e.g. absolute differences in the single scattering albedo under 0.01 for all cases).

On the other hand, the comparison for the sub-set Desert dust II between the retrievals from almucantar and principal plane are systematically much worse than those obtained in the other analyzed cases, in particular the sub-set Desert dust I. The cause of these higher discrepancies has not been identified, however, it seems to be related to the performance of the particular instruments (in this case photometers #233 and #33). Desert dust was identified as the most sensitive aerosol type to errors in the simulations in Sect. 2 (also in the accuracy analysis in Dubovik et al. (2000)).

Finally, this group has been re-analyzed limiting the data set to large  $\theta_s > 50^\circ$ , obtaining significant improvements in the comparison of the retrievals. The analysis for different errors in section 2 also indicates that the differences between almucantar and principal are smaller for larger  $\theta_s$ . In this sense, the differences in the scattering angle range in the two geometries could amplify the discrepancies obtained between the retrievals if they are associated to instrument problems. Accordingly, we can conclude that the Aeronet 2.0 quality criterion on  $\theta_s$  ( $\theta_s > 50^\circ$ ) is also useful in order to reduce the differences that may be associated with the errors during the measurements.

<a href="#">Title Page</a>	
<a href="#">Abstract</a>	<a href="#">Introduction</a>
<a href="#">Conclusions</a>	<a href="#">References</a>
<a href="#">Tables</a>	<a href="#">Figures</a>
<a href="#">◀</a>	<a href="#">▶</a>
<a href="#">◀</a>	<a href="#">▶</a>
<a href="#">Back</a>	<a href="#">Close</a>
<a href="#">Full Screen / Esc</a>	
<a href="#">Printer-friendly Version</a>	
<a href="#">Interactive Discussion</a>	

**Acknowledgements.** We thank the Aeronet, PHOTONS, RIMA and WRC staff for their scientific and technical support. Financial support was provided by: the Spanish CICYT (CGL2009-09740 and CGL2011-23413, CGL2011-13085-E). The research leading to these results has received funding from the European Union Seventh Framework Programme (FP7/2007-2013)

<sup>5</sup> under grant agreement No. 262254 [ACTRIS]. We also thank the Environmental Council of the CyL Regional Government (Consejera de Medio Ambiente, Junta de Castilla y Len) for supporting this research.



- <sup>10</sup> The publication of this article is financed by CNRS-INSU.

## References

- Bohren, C. and Huffman, D.: Absorption and Scattering of Light by Small Particles, John Wiley & Sons Inc, 544 pp., doi:10.1002/9783527618156, 1983. 6859

Cox, C. and Munk, W.: Measurement of the roughness of the sea surface from photographs of the suns glitter, J. Opt. Soc. Am., 44, 838–850, doi:10.1364/JOSA.44.000838, 1954. 6868

D’Almeida, G., Koepke, P., and Shettle, E.: Atmospheric Aerosols: Global Climatology and Radiative Characteristics, A. Deepak Publishing, 561 pp., 1991. 6853

Dubovik, O.: Aerosol retrievals from AERONET sun/sky-radiometers: Overview of inversion principles, products and advances, The Second International Conference of Aerosol Science and Global Change, Hangzhou, China, 2009. 6859

Dubovik, O. and King, M.: A flexible inversion algorithm for retrieval of aerosol optical properties from Sun and sky radiance measurements, J. Geophys. Res.-Atmos., 105, 20673–20696, doi:10.1029/2000JD900282, 2000. 6854, 6856, 6864, 6868

Dubovik, O., Smirnov, A., Holben, B., King, M., Kaufman, Y., Eck, T., and Slutsker, I.: Accuracy assessments of aerosol optical properties retrieved from Aerosol Robotic Network

(AERONET) Sun and sky radiance measurements, *J. Geophys. Res.-Atmos.*, 105, 9791–9806, doi:10.1029/2000JD900040, 2000. 6854, 6856, 6859, 6860, 6886, 6888

Dubovik, O., Holben, B., Eck, T., Smirnov, A., Kaufman, Y., King, M., Tanre, D., and Slutsker, I.: Variability of absorption and optical properties of key aerosol types observed in worldwide locations, *J. Atmos. Sci.*, 59, 590–608, doi:10.1175/1520-0469(2002)059<0590:VOAAOP>2.0.CO;2, 2002. 6854, 6856, 6857, 6880, 6881, 6882, 6885, 6886

Dubovik, O., Sinyuk, A., Lapyonok, T., Holben, B. N., Mishchenko, M., Yang, P., Eck, T., Volten, H., Munoz, O., Veihelmann, B., Van Der Zande, W. J., Leon, J., Sorokin, M., and Slutsker, I.: Application of spheroid models to account for aerosol particle nonsphericity in remote sensing of desert dust, *J. Geophys. Res.-Atmos.*, 111, D11208, doi:10.1029/2005JD006619, 2006. 6854, 6856

Eck, T., Holben, B., Reid, J., Dubovik, O., Smirnov, A., O'Neill, N., Slutsker, I., and Kinne, S.: Wavelength dependence of the optical depth of biomass burning, urban, and desert dust aerosols, *J. Geophys. Res.-Atmos.*, 104, 31333–31349, doi:10.1029/1999JD900923, 1999. 6879

Eck, T., Holben, B., Dubovik, O., Smirnov, A., Goloub, P., Chen, H., Chatenet, B., Gomes, L., Zhang, X., Tsay, S., Ji, Q., Giles, D., and Slutsker, I.: Columnar aerosol optical properties at AERONET sites in central eastern Asia and aerosol transport to the tropical mid-Pacific, *J. Geophys. Res.-Atmos.*, 110, D06202, doi:10.1029/2004JD005274, 2005. 6880

Eck, T. F., Holben, B. N., Sinyuk, A., Pinker, R. T., Goloub, P., Chen, H., Chatenet, B., Li, Z., Singh, R. P., Tripathi, S. N., Reid, J. S., Giles, D. M., Dubovik, O., O'Neill, N. T., Smirnov, A., Wang, P., and Xia, X.: Climatological aspects of the optical properties of fine/coarse mode aerosol mixtures, *J. Geophys. Res.-Atmos.*, 115, D19205, doi:10.1029/2010JD014002, 2010. 6885

Giles, D. M., Holben, B. N., Tripathi, S. N., Eck, T. F., Newcomb, W. W., Slutsker, I., Dickerson, R. R., Thompson, A. M., Mattoo, S., Wang, S.-H., Singh, R. P., Sinyuk, A., and Schafer, J. S.: Aerosol properties over the Indo-Gangetic Plain: A mesoscale perspective from the TIGERZ experiment, *J. Geophys. Res.-Atmos.*, 116, D18203, doi:10.1029/2011JD015809, 2011. 6885

Holben, B., Eck, T., Slutsker, I., Tanre, D., Buis, J., Setzer, A., Vermote, E., Reagan, J., Kaufman, Y., Nakajima, T., Lavenu, F., Jankowiak, I., and Smirnov, A.: AERONET – A federated

## Sensitivity of aerosol retrieval to geometrical configuration

B. Torres et al.

[Title Page](#)

[Abstract](#)

[Introduction](#)

[Conclusions](#)

[References](#)

[Tables](#)

[Figures](#)

◀

▶

◀

▶

[Back](#)

[Close](#)

[Full Screen / Esc](#)

[Printer-friendly Version](#)

[Interactive Discussion](#)



**Sensitivity of aerosol retrieval to geometrical configuration**

B. Torres et al.

[Title Page](#)[Abstract](#)[Introduction](#)[Conclusions](#)[References](#)[Tables](#)[Figures](#)[◀](#)[▶](#)[Back](#)[Close](#)[Full Screen / Esc](#)[Printer-friendly Version](#)[Interactive Discussion](#)

- instrument network and data archive for aerosol characterization, *Remote Sens. Environ.*, 66, 1–16, doi:10.1016/S0034-4257(98)00031-5, 1998. 6854
- Holben, B., Tanre, D., Smirnov, A., Eck, T., Slutsker, I., Abuhaman, N., Newcomb, W., Schafer, J., Chatenet, B., Lavenu, F., Kaufman, Y., Castle, J., Setzer, A., Markham, B., Clark, D., Frouin, R., Halthore, R., Karneli, A., O'Neill, N., Pietras, C., Pinker, R., Voss, K., and Zibordi, G.: An emerging ground-based aerosol climatology: Aerosol optical depth from AERONET, *J. Geophys. Res.-Atmos.*, 106, 12067–12097, doi:10.1029/2001JD900014, 2001. 6885
- Kaufman, Y., Tanre, D., Holben, B., Mattoo, S., Remer, L., Eck, T., Vaughan, J., and Chatenet, B.: Aerosol radiative impact on spectral solar flux at the surface, derived from principal-plane sky measurements, *J. Atmos. Sci.*, 59, 635–646, doi:10.1175/1520-0469(2002)059<0635:ARIOSS>2.0.CO;2, 2002. 6854
- Lucht, W. and Roujean, J.: Considerations in the parametric modeling of BRDF and albedo from multiangular satellite sensor observations, *Remote Sens. Rev.*, 18, 343–379, doi:10.1080/02757250009532395, 2000. 6868
- McCluney, R.: Introduction to Radiometry and Photometry, Artech House Inc., 404 pp., 1994. 6877
- Nakajima, T., Tanaka, M., and Yamauchi, T.: Retrieval of the optical-properties of aerosols from aureola and extinction data, *Appl. Optics*, 22, 2951–2959, 1983. 6854
- Nakajima, T., Tonna, G., Rao, R., Boi, P., Kaufman, Y., and Holben, B.: Use of sky brightness measurements from ground for remote sensing of particulate polydispersions, *Appl. Optics*, 35, 2672–2686, doi:10.1364/AO.35.002672, 1996. 6854, 6855, 6864
- Olmo, F., Quirantes, A., Lara, V., Lyamani, H., and Alados-Arboledas, L.: Aerosol optical properties assessed by an inversion method using the solar principal plane for non-spherical particles, *J. Quant. Spectrosc. Radiat. Trans.*, 109, 1504–1516, 2008. 6854, 6885
- Sinyuk, A., Dubovik, O., Holben, B., Eck, T. F., Breon, F.-M., Martonchik, J., Kahn, R., Diner, D. J., Vermote, E. F., Roger, J.-C., Lapyonok, T., and Slutsker, I.: Simultaneous retrieval of aerosol and surface properties from a combination of AERONET and satellite data, *Remote Sens. Environ.*, 107, 90–108, doi:10.1016/j.rse.2006.07.022, 2007. 6864
- Smirnov, A., Holben, B., Eck, T., Slutsker, I., Chatenet, B., and Pinker, R.: Diurnal variability of aerosol optical depth observed at AERONET (Aerosol Robotic Network) sites, *Geophys. Res. Lett.*, 29, 2115, doi:10.1029/2002GL016305, 2002. 6885
- Solomon, S., Qin, D., Manning, M., Chen, Z., Marquis, M., Averyt, K. B., Tignor M., and Miller, H. L.: Technical Summary, in: Climate Change 2007: The Physical Science Basis Contribution

## Sensitivity of aerosol retrieval to geometrical configuration

B. Torres et al.

<a href="#">Title Page</a>	<a href="#">Abstract</a>	<a href="#">Introduction</a>
<a href="#">Conclusions</a>	<a href="#">References</a>	
<a href="#">Tables</a>	<a href="#">Figures</a>	
<a href="#">◀</a>	<a href="#">▶</a>	
<a href="#">◀</a>	<a href="#">▶</a>	
<a href="#">Back</a>	<a href="#">Close</a>	
<a href="#">Full Screen / Esc</a>		

[Printer-friendly Version](#)

[Interactive Discussion](#)



## Sensitivity of aerosol retrieval to geometrical configuration

B. Torres et al.

[Title Page](#)

[Abstract](#)

[Introduction](#)

[Conclusions](#)

[References](#)

[Tables](#)

[Figures](#)

◀

▶

[Back](#)

[Close](#)

[Full Screen / Esc](#)

[Printer-friendly Version](#)

[Interactive Discussion](#)



**Table 1.** Description of aerosol properties used for simulating the radiance measurements. The first row specifies the parameters describing the size distribution which is modeled as a bimodal lognormal function:  $C_{V_i}$  [ $\mu\text{m}^3 \mu\text{m}^{-2}$ ],  $r_{V_i}$  [ $\mu\text{m}$ ] and  $\sigma_{V_i}$ . Refractive index and the sphericity parameter are also parts of the input. Single scattering albedo and aerosol optical depth, for each wavelength, are shown as the output after applying the forward model.

Biomass Burning (Zambia)								
INPUT	$\tau_{a_{ref}}$ (440)	$r_{V_f}$	$\sigma_{V_f}$	$C_{V_f}$	$r_{V_c}$	$\sigma_{V_c}$	$C_{V_c}$	$Sph.$
- Zamb1 -	0.400	0.130	0.400	0.048	3.504	0.730	0.004	100
- Zamb2 -	0.800	0.140	0.400	0.096	3.788	0.730	0.007	100
	$n(440)$	$n(670)$	$n(870)$	$n(1020)$	$k(440)$	$k(670)$	$k(870)$	$k(1020)$
- Zamb1 -	1.5100	1.5100	1.5100	1.5100	0.0210	0.0210	0.0210	0.0210
- Zamb2 -	1.5100	1.5100	1.5100	1.5100	0.0210	0.0210	0.0210	0.0210
OUTPUT	$\tau_a$ (440)	$\tau_a$ (670)	$\tau_a$ (870)	$\tau_a$ (1020)	$\omega_o$ (440)	$\omega_o$ (670)	$\omega_o$ (870)	$\omega_o$ (1020)
- Zamb1 -	0.416	0.184	0.107	0.078	0.8778	0.8290	0.7811	0.7467
- Zamb2 -	0.872	0.397	0.232	0.167	0.8827	0.8402	0.7958	0.7620
Urban (GSFC)								
INPUT	$\tau_{a_{ref}}$ (440)	$r_{V_f}$	$\sigma_{V_f}$	$C_{V_f}$	$r_{V_c}$	$\sigma_{V_c}$	$C_{V_c}$	$Sph.$
- GSFC1 -	0.200	0.142	0.380	0.030	3.128	0.790	0.018	100
- GSFC2 -	0.500	0.175	0.380	0.075	3.275	0.790	0.030	100
	$n(440)$	$n(670)$	$n(870)$	$n(1020)$	$k(440)$	$k(670)$	$k(870)$	$k(1020)$
- GSFC1 -	1.4100	1.4100	1.4100	1.4100	0.0030	0.0030	0.0030	0.0030
- GSFC2 -	1.4100	1.4100	1.4100	1.4100	0.0030	0.0030	0.0030	0.0030
OUTPUT	$\tau_a$ (440)	$\tau_a$ (670)	$\tau_a$ (870)	$\tau_a$ (1020)	$\omega_o$ (440)	$\omega_o$ (670)	$\omega_o$ (870)	$\omega_o$ (1020)
- GSFC1 -	0.195	0.083	0.048	0.036	0.9718	0.9588	0.9476	0.9404
- GSFC2 -	0.559	0.254	0.145	0.102	0.9771	0.9691	0.9604	0.9535
Desert Dust (Solar Village)								
INPUT	$\tau_{a_{ref}}$ (1020)	$r_{V_f}$	$\sigma_{V_f}$	$C_{V_f}$	$r_{V_c}$	$\sigma_{V_c}$	$C_{V_c}$	$Sph.$
- SolV1 -	0.300	0.120	0.400	0.026	2.320	0.600	0.274	0
- SolV2 -	0.500	0.120	0.400	0.030	2.320	0.600	0.470	0
	$n(440)$	$n(670)$	$n(870)$	$n(1020)$	$k(440)$	$k(670)$	$k(870)$	$k(1020)$
- SolV1 -	1.5600	1.5600	1.5600	1.5600	0.0029	0.0013	0.0010	0.0010
- SolV2 -	1.5600	1.5600	1.5600	1.5600	0.0029	0.0013	0.0010	0.0010
OUTPUT	$\tau_a$ (440)	$\tau_a$ (670)	$\tau_a$ (870)	$\tau_a$ (1020)	$\omega_o$ (440)	$\omega_o$ (670)	$\omega_o$ (870)	$\omega_o$ (1020)
- SolV1 -	0.483	0.371	0.344	0.332	0.9300	0.9664	0.9772	0.9794
- SolV2 -	0.707	0.591	0.568	0.557	0.9209	0.9647	0.9768	0.9793

## Sensitivity of aerosol retrieval to geometrical configuration

B. Torres et al.

**Table 2.** Retrieved aerosol optical parameters considering different number of layers. The aerosol type considered has been the urban aerosol at  $\theta_s = 75^\circ$  with the aerosol vertical distribution centered at the surface.

	440 nm			670 nm			870 nm			1020 nm		
	<i>n</i>	<i>k</i>	$\omega_o$									
Reference	1.410	0.003	0.977	1.410	0.003	0.969	1.410	0.003	0.960	1.410	0.003	0.954
1-Layer	1.519	0.003	0.977	1.494	0.003	0.970	1.487	0.003	0.961	1.484	0.003	0.955
2-Layers	1.439	0.003	0.977	1.431	0.003	0.969	1.428	0.003	0.960	1.427	0.003	0.953
5-Layers	1.411	0.003	0.976	1.411	0.003	0.968	1.411	0.003	0.959	1.412	0.003	0.952
2-Layers-2km	1.410	0.003	0.976	1.410	0.003	0.968	1.411	0.003	0.959	1.411	0.003	0.952
2-Layers-4km	1.422	0.003	0.977	1.419	0.003	0.969	1.418	0.003	0.960	1.418	0.003	0.953
2-Layers-6km	1.440	0.003	0.978	1.433	0.003	0.970	1.431	0.003	0.961	1.431	0.003	0.954

<a href="#">Title Page</a>	
<a href="#">Abstract</a>	<a href="#">Introduction</a>
<a href="#">Conclusions</a>	<a href="#">References</a>
<a href="#">Tables</a>	<a href="#">Figures</a>
<a href="#"></a>	<a href="#"></a>
<a href="#"></a>	<a href="#"></a>
<a href="#">Full Screen / Esc</a>	

[Printer-friendly Version](#)

[Interactive Discussion](#)



## Sensitivity of aerosol retrieval to geometrical configuration

B. Torres et al.

**Table 3.** Values of  $\rho_o(\lambda)$ ,  $\kappa(\lambda)$  and  $\Theta(\lambda)$  used to approximates the surface reflectance by a Bi-directional Reflectance Function (BDRF) in the sites used in the simulations: Mongu, Goddard and Solar Village.

	440 nm			670 nm			870 nm			1020 nm		
	$\rho_o$	$\kappa$	$\Theta$									
Mongu (dry season)	0.064	0.026	0.010	0.147	0.076	0.024	0.274	0.173	0.029	0.311	0.196	0.033
Goddard (winter)	0.032	0.008	0.003	0.092	0.035	0.011	0.209	0.234	0.033	0.232	0.227	0.032
Solar Village	0.161	0.074	0.024	0.405	0.217	0.057	0.445	0.272	0.037	0.479	0.293	0.040

[Title Page](#)[Abstract](#)[Introduction](#)[Conclusions](#)[References](#)[Tables](#)[Figures](#)[Full Screen / Esc](#)[Printer-friendly Version](#)[Interactive Discussion](#)

## Sensitivity of aerosol retrieval to geometrical configuration

B. Torres et al.

[Title Page](#)

[Abstract](#)

[Introduction](#)

[Conclusions](#)

[References](#)

[Tables](#)

[Figures](#)

[|◀](#)

[▶|](#)

[◀](#)

[▶](#)

[Back](#)

[Close](#)

[Full Screen / Esc](#)

[Printer-friendly Version](#)

[Interactive Discussion](#)



**Table 4.** Description of the data used for the comparison between almucantar and principal plane retrievals for the different sites.

Biomass burning (Mongu)				Urban (Beijing)			
Photometer	Date	N° pairs	$\langle \tau_a(440) \rangle$	Photometer	Date	N° pairs	$\langle \tau_a(440) \rangle$
#36	09-08-2009	4	0.34	#14	08-01-2003	6	1.19
	12-08-2009	7	0.63		08-02-2003	5	1.79
	16-07-2009	5	0.71		12-02-2005	4	1.09
	01-10-2004	4	0.37		03-11-2004	5	1.78
#65	25-07-2004	6	0.61	#111	27-08-2006	6	0.99
	17-09-2004	6	0.78		02-11-2005	5	1.81
	30-07-2003	5	0.45		20-02-2007	6	1.19
#11	18-08-2003	6	0.68	#73	05-11-2007	6	1.95
	14-08-2003	6	0.72		15-01-2009	4	0.46
	02-08-2006	6	0.42		17-09-2009	4	1.72
#152	25-07-2006	4	0.53	#246	05-03-2011	4	1.28
	18-08-2006	6	0.73		28-08-2011	4	1.74
Desert dust I (Solar Village)				Desert dust II (Solar Village)			
Photometer	Date	No. pairs	$\langle \tau_a(440) \rangle$	Photometer	Date	N° pairs	$\langle \tau_a(440) \rangle$
#65	18-09-2002	6	0.38	#233	25-04-2008	7	0.36
	02-04-2003	5	0.48		28-05-2008	6	0.51
	11-09-2002	5	0.64		29-07-2008	4	0.70
	20-10-2005	6	0.32		04-06-2004	7	0.33
#185	19-10-2005	7	0.41	#33	22-05-2004	4	0.46
	19-06-2006	5	0.54		18-05-2004	5	0.71
	24-08-2010	5	0.39				
#95	09-10-2010	5	0.48				
	26-08-2010	6	0.73				

**Table 5.** Mean values and standard deviations obtained for the single scattering albedo and the refractive index in the analyzed days using only almucantar geometry.

	$\omega(\lambda)$					$n(\lambda)$					$k(\lambda)$					
Wavelength [nm]	440	670	870	1020	440	670	870	1020	440	670	870	1020	440	670	870	1020
Bio. Burn. mean	0.85	0.81	0.78	0.76	1.53	1.53	1.54	1.54	0.032	0.032	0.030	0.027				
(Mongu) std	0.03	0.05	0.05	0.05	0.04	0.03	0.03	0.03	0.012	0.013	0.012	0.011				
Urban mean	0.92	0.92	0.90	0.89	1.48	1.49	1.49	1.49	0.016	0.011	0.012	0.012				
(Beijing) std	0.05	0.03	0.04	0.04	0.03	0.03	0.04	0.03	0.009	0.005	0.005	0.005				
Desert dust mean	0.90	0.92	0.94	0.94	1.51	1.54	1.54	1.54	0.006	0.004	0.004	0.004				
(Solar Vil.) std	0.02	0.03	0.03	0.03	0.05	0.03	0.03	0.03	0.003	0.003	0.002	0.002				

[Title Page](#)  
 [Abstract](#)   [Introduction](#)  
 [Conclusions](#)   [References](#)  
 [Tables](#)   [Figures](#)  
 [◀](#)   [▶](#)  
 [◀](#)   [▶](#)  
 [Back](#)   [Close](#)  
 [Full Screen / Esc](#)

[Printer-friendly Version](#)

[Interactive Discussion](#)



**Sensitivity of aerosol retrieval to geometrical configuration**

B. Torres et al.

**Table 6.** Mean values of the particle volume concentration  $C_{Vi}$ , the median radius  $r_{Vi}$ , and the standard deviation  $\sigma_{Vi}$  for each mode of the volume particle size distribution for the defined groups Desert dust I and Desert dust II.

	$C_{Vf}$	$r_{Vf}$	$\sigma_{Vf}$	$C_{Vc}$	$r_{Vc}$	$\sigma_{Vc}$
Desert dust I	$0.03 \pm 0.01$	$0.15 \pm 0.02$	$0.47 \pm 0.05$	$0.25 \pm 0.10$	$2.47 \pm 0.18$	$0.62 \pm 0.03$
Desert dust II	$0.03 \pm 0.02$	$0.17 \pm 0.04$	$0.60 \pm 0.07$	$0.25 \pm 0.07$	$2.09 \pm 0.28$	$0.57 \pm 0.06$

[Abstract](#) [Introduction](#)  
[Conclusions](#) [References](#)  
[Tables](#) [Figures](#)[◀](#) [▶](#)  
[◀](#) [▶](#)  
[Back](#) [Close](#)  
[Full Screen / Esc](#)

## Sensitivity of aerosol retrieval to geometrical configuration

B. Torres et al.

**Table 7.** Mean values and the standard deviations of the absolute differences (with sign principal plane minus almucantar) for the optical parameters found for the data set Desert dust II.

	Total differences											
	$\omega(\lambda)$				$n(\lambda)$				$k(\lambda)$			
Wavelength [nm]	440	670	870	1020	440	670	870	1020	440	670	870	1020
All	mean	0.03	0.03	0.03	0.02	0.03	0.03	0.03	-0.004	-0.003	-0.003	-0.002
data	std	0.05	0.05	0.04	0.03	0.06	0.05	0.05	0.06	0.006	0.005	0.004
$\theta_s >$	mean	0.01	0.00	0.00	0.00	0.01	0.01	0.01	0.01	-0.001	-0.000	-0.000
30°	std	0.02	0.02	0.02	0.01	0.02	0.02	0.02	0.02	0.003	0.002	0.002
$\theta_s >$	mean	-0.00	-0.01	-0.00	-0.00	0.01	0.01	0.01	0.01	0.001	0.000	0.000
50°	std	0.01	0.01	0.01	0.01	0.02	0.02	0.02	0.02	0.001	0.001	0.001

<a href="#">Title Page</a>	<a href="#">Abstract</a>	<a href="#">Introduction</a>
<a href="#">Conclusions</a>	<a href="#">References</a>	
<a href="#">Tables</a>	<a href="#">Figures</a>	
<a href="#">◀</a>	<a href="#">▶</a>	
<a href="#">◀</a>	<a href="#">▶</a>	
<a href="#">Back</a>	<a href="#">Close</a>	
<a href="#">Full Screen / Esc</a>		

<a href="#">Printer-friendly Version</a>
<a href="#">Interactive Discussion</a>

**Sensitivity of aerosol retrieval to geometrical configuration**

B. Torres et al.

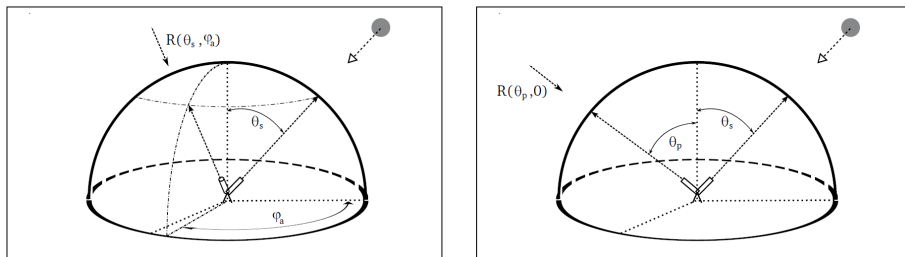


**Fig. 1.** Figures describing the two geometries used within Aeronet network for the measurements of the sky radiances: on the left, the almucantar is represented while the principal plane appears on the right.

[Title Page](#)[Abstract](#)[Introduction](#)[Conclusions](#)[References](#)[Tables](#)[Figures](#)[|◀](#)[▶|](#)[Back](#)[Close](#)[Full Screen / Esc](#)[Printer-friendly Version](#)[Interactive Discussion](#)

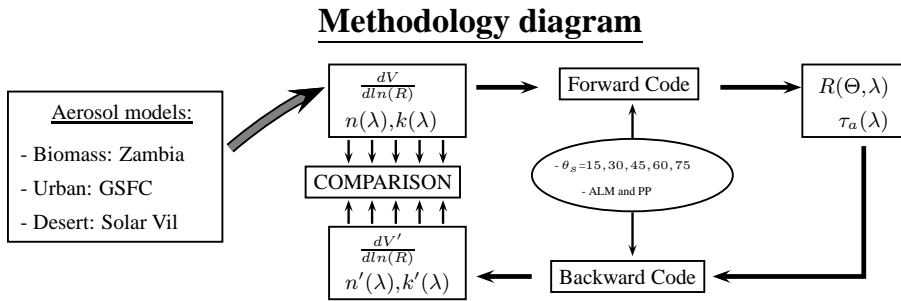


**Fig. 2.** Methodology diagram followed to carry out the self-consistency test of the used code for different aerosol types, solar zenith angles and geometries for measuring the sky radiance.

## Sensitivity of aerosol retrieval to geometrical configuration

B. Torres et al.

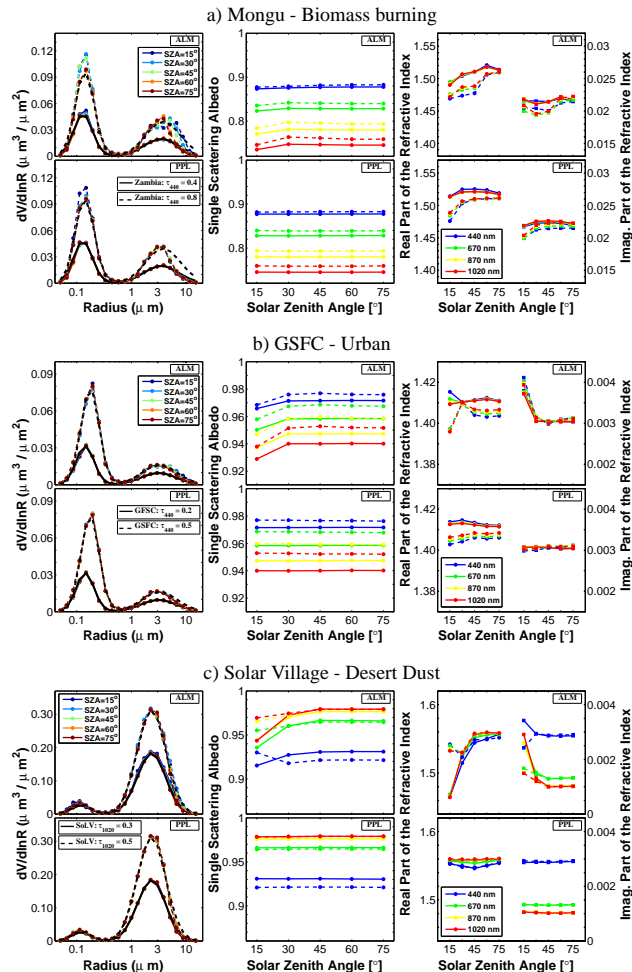


**Fig. 3.** Please see caption on next page.

## Sensitivity of aerosol retrieval to geometrical configuration

B. Torres et al.

**Fig. 3.** Summary of the aerosol retrievals obtained in the self-consistency test using three aerosol types: biomass burning aerosol (**a**), urban aerosol (**b**) and desert dust aerosol (**c**) with two different AOD utilized as reference in each case (solid line used for the case with smallest aerosol load and dashed line for the largest). For every subfigure, almucantar results are shown in the upper part whereas principal plane results are presented in the bottom part. Figures on the left correspond to size distribution results. Figures in the center illustrate the results for the single scattering albedo, and figures on the right describe the results for the complex refractive index.

[Title Page](#)

[Abstract](#)

[Introduction](#)

[Conclusions](#)

[References](#)

[Tables](#)

[Figures](#)

◀

▶

[Back](#)

[Close](#)

[Full Screen / Esc](#)

[Printer-friendly Version](#)

[Interactive Discussion](#)



## Sensitivity of aerosol retrieval to geometrical configuration

B. Torres et al.

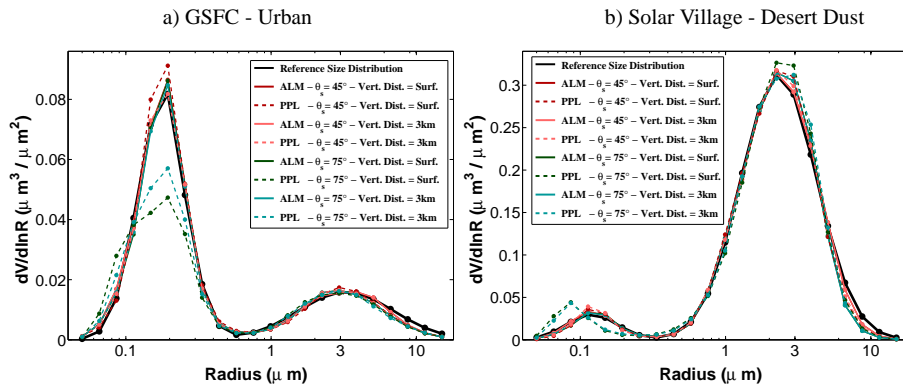


**Fig. 4.** Aerosol size distributions retrieved in the study of the influence on the aerosol vertical profiles. Using the aerosol properties of urban (**a**) and desert dust (**b**), radiance measurements have been previously simulated for the two geometries, almucantar (solid line) and principal plane (dashed line), considering 30 layers in the atmosphere. During the retrieving process, only one layer has been used in the four analyzed cases:  $\theta_s = 45^\circ$  and vertical profile centered in the earth surface (red lines),  $\theta_s = 45^\circ$  and vertical profile centered at  $h = 3\text{ km}$  (pink lines),  $\theta_s = 75^\circ$  and vertical profile centered in the earth surface (green lines),  $\theta_s = 75^\circ$  and vertical profile centered at  $h=3\text{ km}$  (blue lines).

- [Title Page](#)
- [Abstract](#) [Introduction](#)
- [Conclusions](#) [References](#)
- [Tables](#) [Figures](#)
- [◀](#) [▶](#)
- [Back](#) [Close](#)
- [Full Screen / Esc](#)

- [Printer-friendly Version](#)
- [Interactive Discussion](#)

## Sensitivity of aerosol retrieval to geometrical configuration

B. Torres et al.

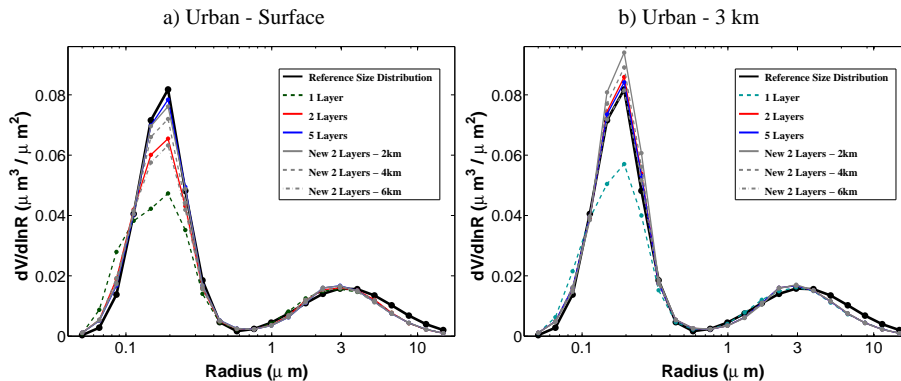


**Fig. 5.** Aerosol size distributions retrieved considering more than one layer for principal plane geometry in the case of urban aerosol at  $\theta_s = 75^\circ$ . **(a)** contains the results for the case with aerosol concentration profile median height at ground level, and **(b)** for the case with the maximum at 3 km. Red and blue lines represent the cases for 2-layers and 5-layers respectively, being this layers equidistant in pressure and adding the description of the aerosol vertical profile. Gray lines represent the alternative solutions when the vertical profile is unknown: solid line when the border between the layers aerosol-non aerosol is fixed at 2 km, dash line when the border is at 4 km and dash-dotted when is at 6 km.

[Title Page](#)

[Abstract](#)

[Introduction](#)

[Conclusions](#)

[References](#)

[Tables](#)

[Figures](#)

◀

▶

[Back](#)

[Close](#)

[Full Screen / Esc](#)

[Printer-friendly Version](#)

[Interactive Discussion](#)

## Sensitivity of aerosol retrieval to geometrical configuration

B. Torres et al.

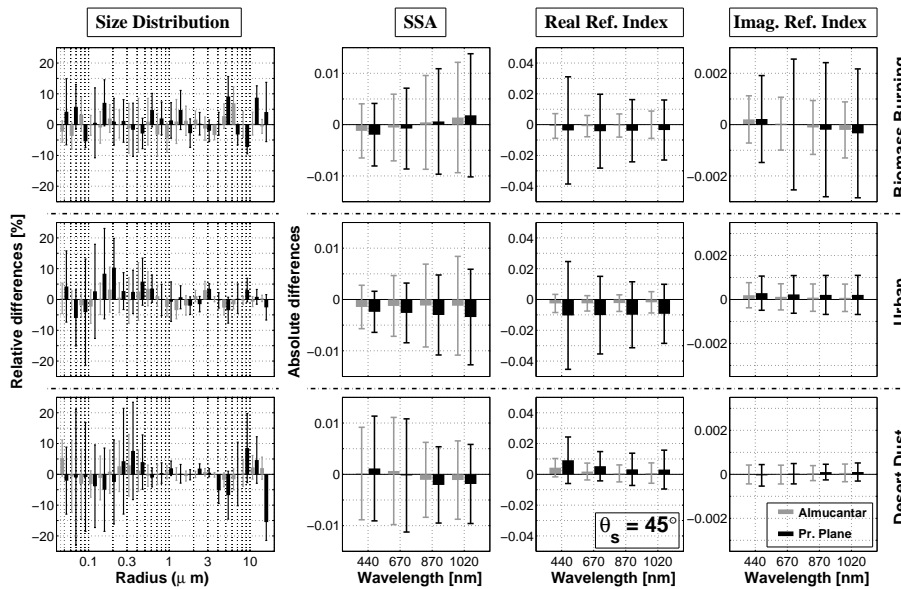


**Fig. 6.** Means and the standard deviations of the differences between the 200 retrievals, where gaussian errors are introduced in the BDRF parameters, and the non-error case at  $\theta_s = 45^\circ$ . Figures at the top correspond to biomass burning aerosol, in the middle to urban aerosol and at the bottom to desert dust aerosol. Relative differences are used for the analyses of the size distribution (figures in the left), while the differences in the optical parameters are provided in absolute terms. Results are shown for almucantar (gray-color) and for principal plane (black-color).

[Title Page](#)

[Abstract](#) [Introduction](#)

[Conclusions](#) [References](#)

[Tables](#) [Figures](#)



[Full Screen / Esc](#)

[Printer-friendly Version](#)

[Interactive Discussion](#)

## Sensitivity of aerosol retrieval to geometrical configuration

B. Torres et al.

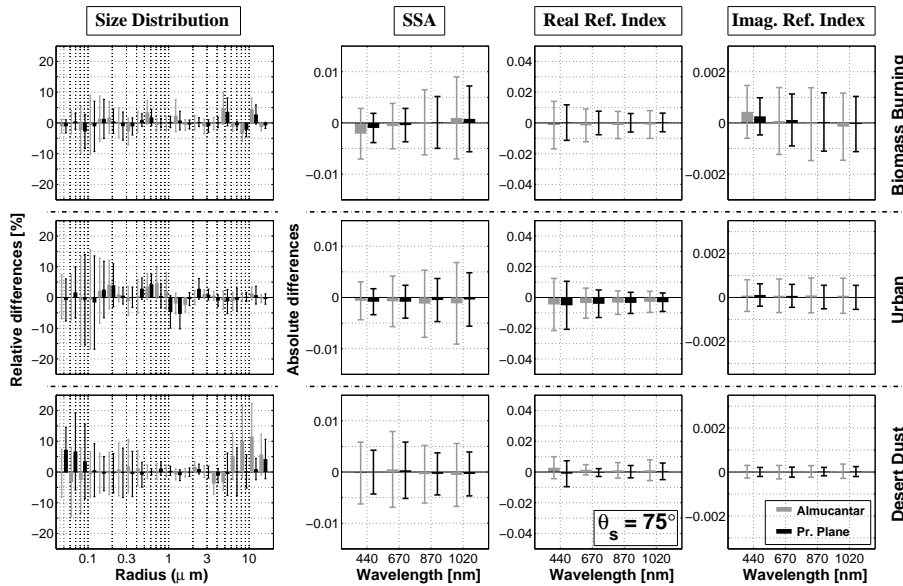


**Fig. 7.** Means and the standard deviations of the differences between the 200 retrievals, where gaussian errors are introduced in the BDGF parameters, and the non-error case at  $\theta_s = 75^\circ$ . Figures at the top correspond to biomass burning aerosol, in the middle to urban aerosol and at the bottom to desert dust aerosol. Relative differences are used for the analyses of the size distribution (figures in the left), while the differences in the optical parameters are provided in absolute terms. Results are shown for almucantar (gray-color) and for principal plane (black-color).

[Title Page](#)

[Abstract](#)

[Introduction](#)

[Conclusions](#)

[References](#)

[Tables](#)

[Figures](#)

◀

▶

◀

▶

[Back](#)

[Close](#)

[Full Screen / Esc](#)

[Printer-friendly Version](#)

[Interactive Discussion](#)

## Sensitivity of aerosol retrieval to geometrical configuration

B. Torres et al.

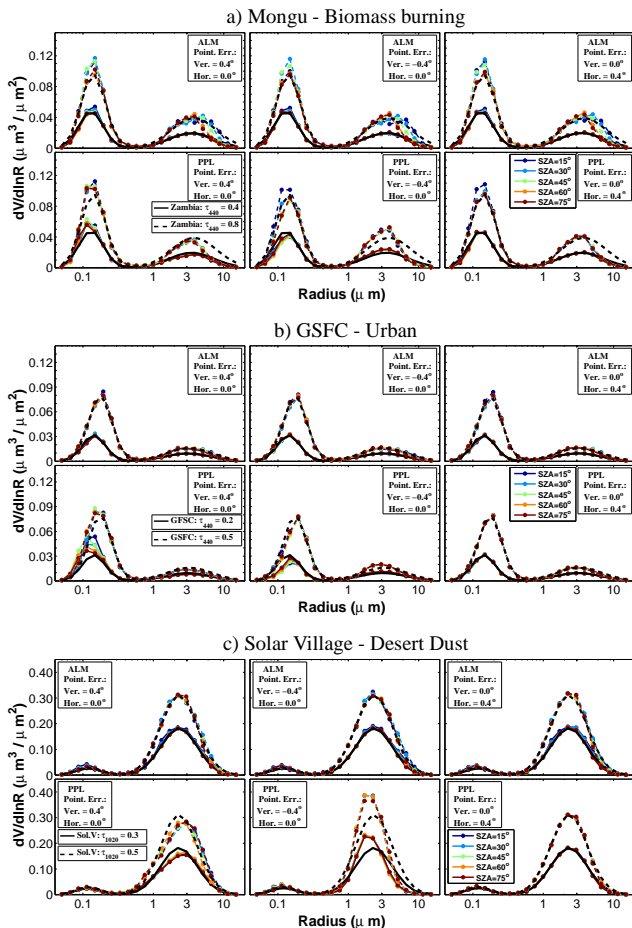


**Fig. 8.** Please see caption on next page.

## Sensitivity of aerosol retrieval to geometrical configuration

B. Torres et al.

**Fig. 8.** Retrieved size distributions after simulating a pointing error of  $0.4^\circ$  in three different aerosol types: biomass burning aerosol (**a**), urban aerosol (**b**) and desert dust aerosol (**c**) with two different AOD as reference in each case (solid line used for the case with smallest aerosol load and dashed line for the largest). In each of the figures, subfigures on top show results from almucantars and at the bottom from principal planes. Subfigures on the left correspond to retrievals with vertical errors, and on the right, to horizontal errors. Colors indicate the solar zenith angle: dark blue for  $\theta_s = 15^\circ$ , light blue for  $\theta_s = 30^\circ$ , green for  $\theta_s = 45^\circ$ , orange for  $\theta_s = 60^\circ$  and brown for  $\theta_s = 75^\circ$  while black is used for the original size distributions.

[Title Page](#)

[Abstract](#)

[Introduction](#)

[Conclusions](#)

[References](#)

[Tables](#)

[Figures](#)

[◀](#)

[▶](#)

[Back](#)

[Close](#)

[Full Screen / Esc](#)

[Printer-friendly Version](#)

[Interactive Discussion](#)



## Sensitivity of aerosol retrieval to geometrical configuration

B. Torres et al.

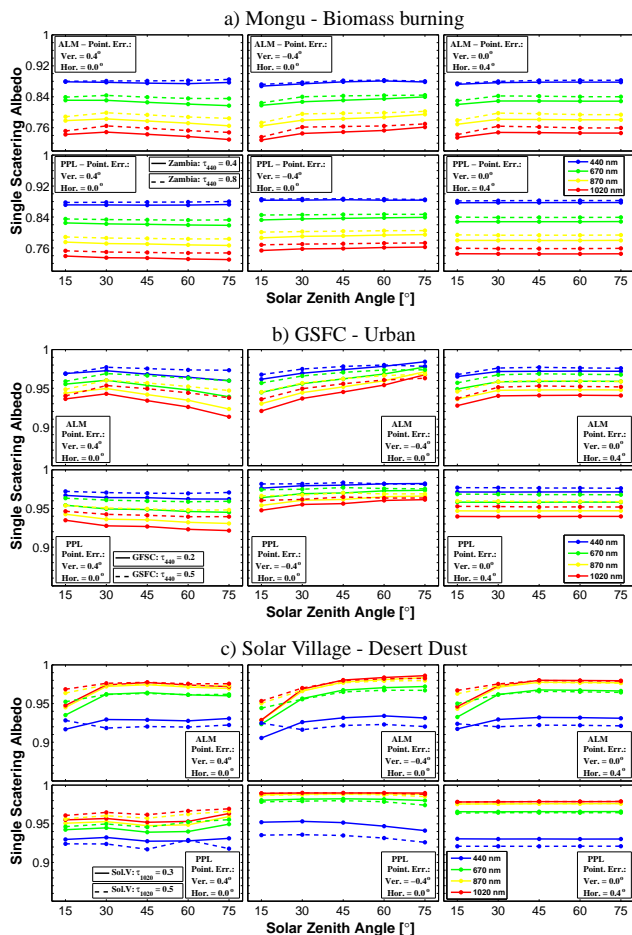


**Fig. 9.** Please see caption on next page.

## Sensitivity of aerosol retrieval to geometrical configuration

B. Torres et al.

**Fig. 9.** Retrieved single scattering albedo after simulating a pointing error of  $0.4^\circ$  in three different aerosol types: biomass burning aerosol (**a**), urban aerosol (**b**) and desert dust aerosol (**c**) with two different AOD as reference in each case (solid line used for the case with smallest aerosol load and dashed line for the largest). In each of the figures, subfigures on top show results from almucantars and at the bottom from principal planes. Subfigures on the left correspond to retrievals with vertical errors, and on the right, to horizontal errors. Colors indicate the wavelength: blue for 440 nm, green for 670 nm, yellow for 870 nm and red for 1020 nm. Y-Axes express the real refractive index (on the left) and the imaginary refractive index (on the right)

[Title Page](#)

[Abstract](#)

[Introduction](#)

[Conclusions](#)

[References](#)

[Tables](#)

[Figures](#)

◀

▶

◀

▶

Back

Close

[Full Screen / Esc](#)

[Printer-friendly Version](#)

[Interactive Discussion](#)



## Sensitivity of aerosol retrieval to geometrical configuration

B. Torres et al.

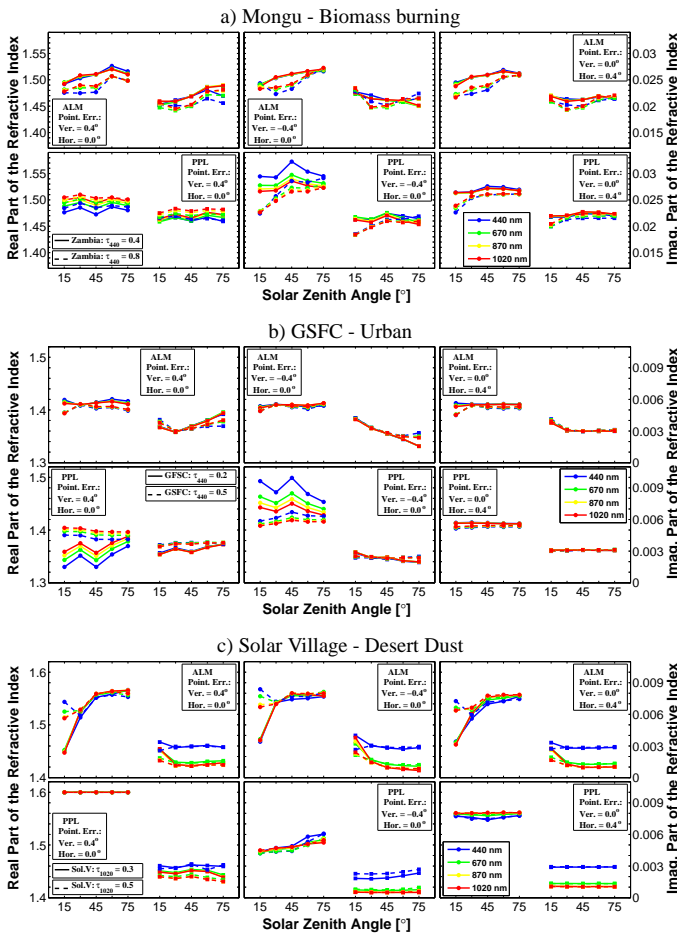


**Fig. 10.** Please see caption on next page.

[Title Page](#)

[Abstract](#)

[Introduction](#)

[Conclusions](#)

[References](#)

[Tables](#)

[Figures](#)

◀

▶

[Back](#)

[Close](#)

[Full Screen / Esc](#)

## Sensitivity of aerosol retrieval to geometrical configuration

B. Torres et al.

**Fig. 10.** Retrieved refractive index after simulating a pointing error of  $0.4^\circ$  in three different aerosol types: biomass burning aerosol (**a**), urban aerosol (**b**) and desert dust aerosol (**c**) with two different AOD as reference in each case (solid line used for the case with smallest aerosol load and dashed line for the largest). In each of the figures, subfigures on top show results from almucantars and at the bottom from principal planes. Subfigures on the left correspond to retrievals with vertical errors, and on the right, to horizontal errors. Colors indicate the wavelength: blue for 440 nm, green for 670 nm, yellow for 870 nm and red for 1020 nm. Y-Axes express the real refractive index (on the left) and the imaginary refractive index (on the right)

[Title Page](#)

[Abstract](#)

[Introduction](#)

[Conclusions](#)

[References](#)

[Tables](#)

[Figures](#)

◀

▶

[Back](#)

[Close](#)

[Full Screen / Esc](#)

[Printer-friendly Version](#)

[Interactive Discussion](#)



## Sensitivity of aerosol retrieval to geometrical configuration

B. Torres et al.

[Title Page](#)

[Abstract](#)

[Introduction](#)

[Conclusions](#)

[References](#)

[Tables](#)

[Figures](#)

◀

▶

◀  
Back

▶  
Close

[Full Screen / Esc](#)

[Printer-friendly Version](#)

[Interactive Discussion](#)

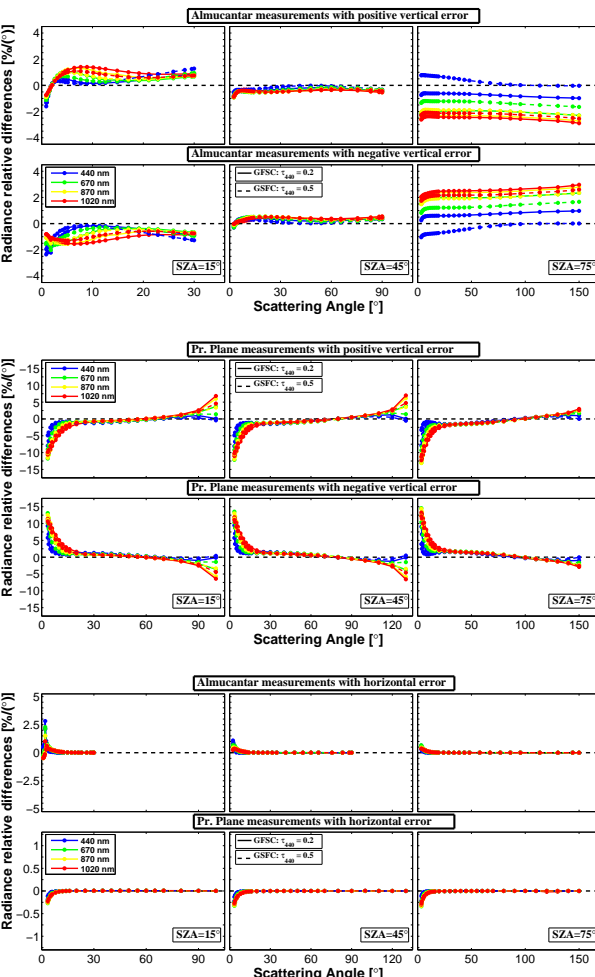


**Fig. 11.** Please see caption on next page.

## Sensitivity of aerosol retrieval to geometrical configuration

B. Torres et al.

**Fig. 11.** Radiance relative differences obtained simulating a pointing error of  $0.4^\circ$ . GSFC aerosol was taken as example using two different AOD:  $\tau_{440} = 0.2$  (solid line) and  $\tau_{440} = 0.5$  (dashed line). Figures in the upper part correspond to vertical errors for almucantar and principal plane (4 subfigure due to double sign). On the bottom, the effects of horizontal errors are represented. From left to right,  $\theta_s$  increases for the different figures.

[Title Page](#)

[Abstract](#)

[Introduction](#)

[Conclusions](#)

[References](#)

[Tables](#)

[Figures](#)

[◀](#)

[▶](#)

[◀](#)

[▶](#)

[Back](#)

[Close](#)

[Full Screen / Esc](#)

[Printer-friendly Version](#)

[Interactive Discussion](#)



# Sensitivity of aerosol retrieval to geometrical configuration

B. Torres et al.

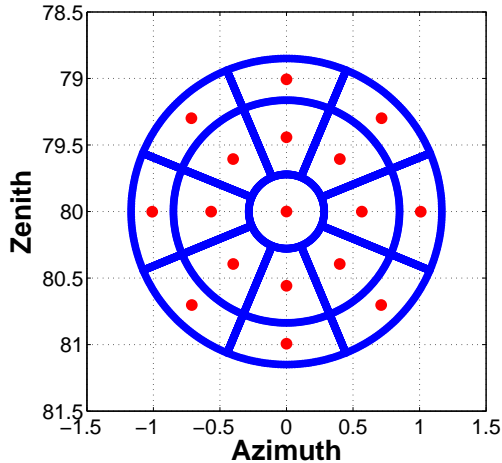


**Fig. 12.** Representation of the 17 point-scheme followed to simulate the effects of a finite field of view on the radiance measurements. In the example the field of view is  $2.4^\circ$  and  $\theta_s = 80^\circ$ .

Title Page

## Abstract

Introduction

## Conclusions

## References

## Tables

## Figures

1

1

1

1

Back

**Close**

Full Screen / Esc

ANSWER



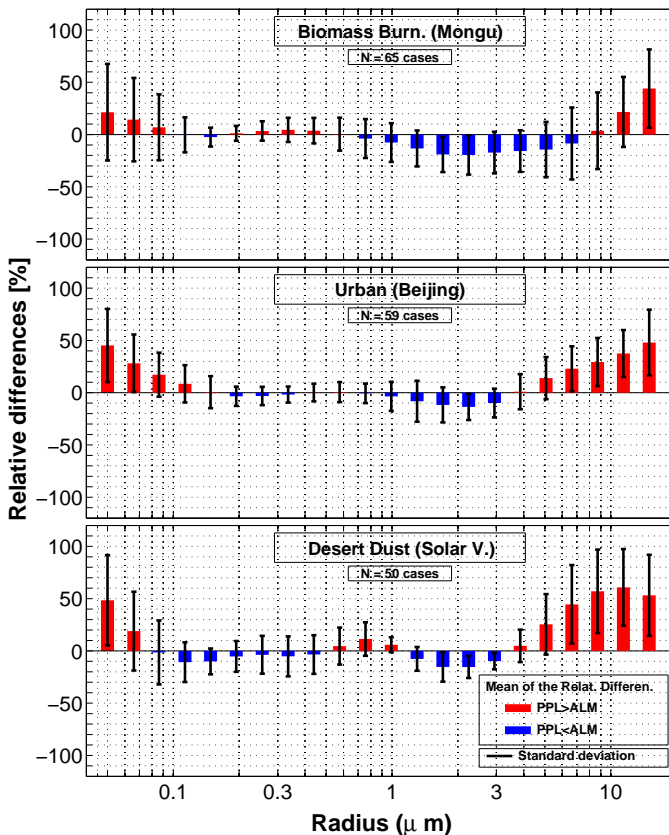


**Fig. 13.** Relative differences found in the size distribution between the inversion obtained by almucantar and principal planes for the three analyzed cases (data description in Table 4): biomass burning (upper part of the figure) urban (central part of the figure) and desert dust (lower part of the figure, only data from the first set (called Desert dust I)).

## Sensitivity of aerosol retrieval to geometrical configuration

B. Torres et al.

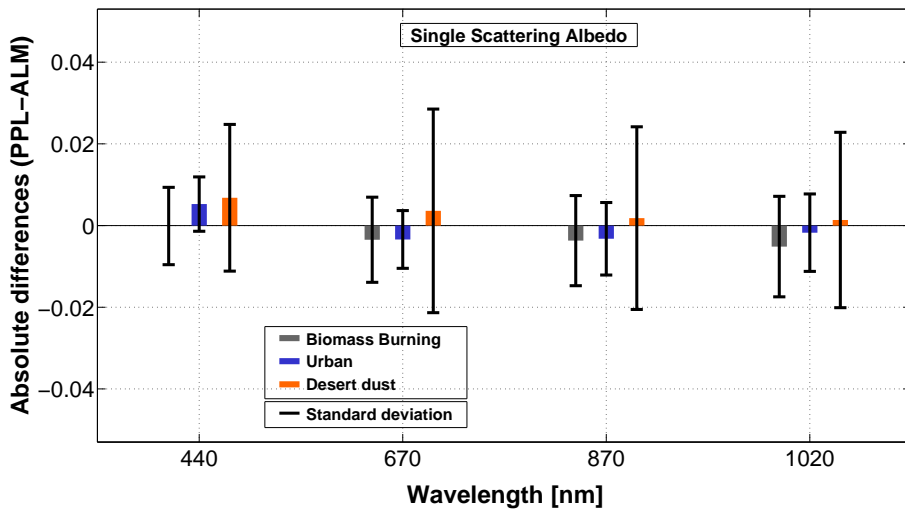


**Fig. 14.** Absolute differences (with sign) found in the single scattering albedo between the inversion obtained by almucantar and principal planes for the three analyzed cases (Table 4): biomass burning (gray), urban (blue) and desert dust (orange, only data from the first set (called Desert dust I)). Bars indicate the standard deviation of the differences

Title Page

## Abstract

Introduction

## Conclusions

## References

Tables

## Figures

1

1

1

1

Back

**Close**

Full Screen / Esc

[Printer friendly version](#)

## Interactive Discussion

## Sensitivity of aerosol retrieval to geometrical configuration

B. Torres et al.

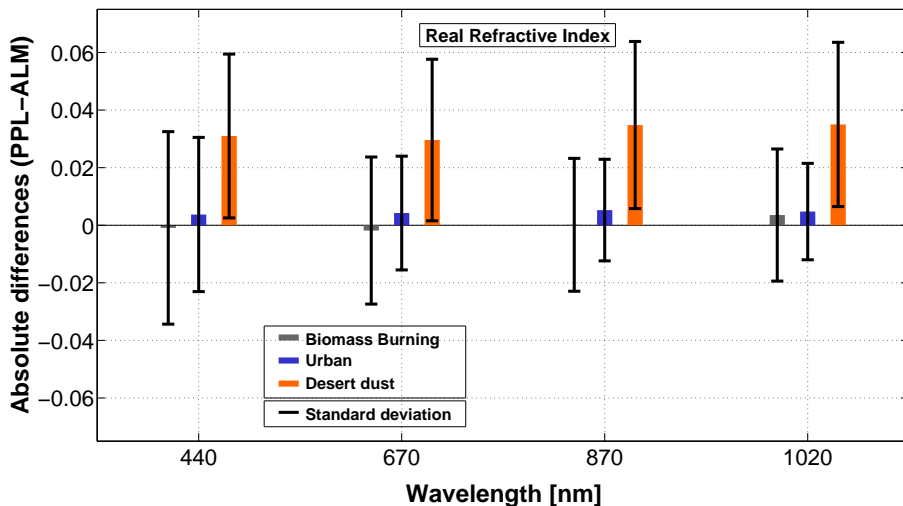


**Fig. 15.** Absolute differences (with sign) found in the real part of the refractive index between the inversion obtained by almucantar and principal planes for the three analyzed cases (Table 4): biomass burning (gray), urban(blue) and desert dust (orange, only data from the first set (called Desert dust I)). Bars indicate the standard deviation of the differences.

Title Page

## Abstract

Introduction

## Conclusions

References

Tables

## Figures

1

1

1

1

Back

Close

Full Screen / Esc

[Printer-friendly Version](#)

## Interactive Discussion



**Sensitivity of aerosol retrieval to geometrical configuration**

B. Torres et al.

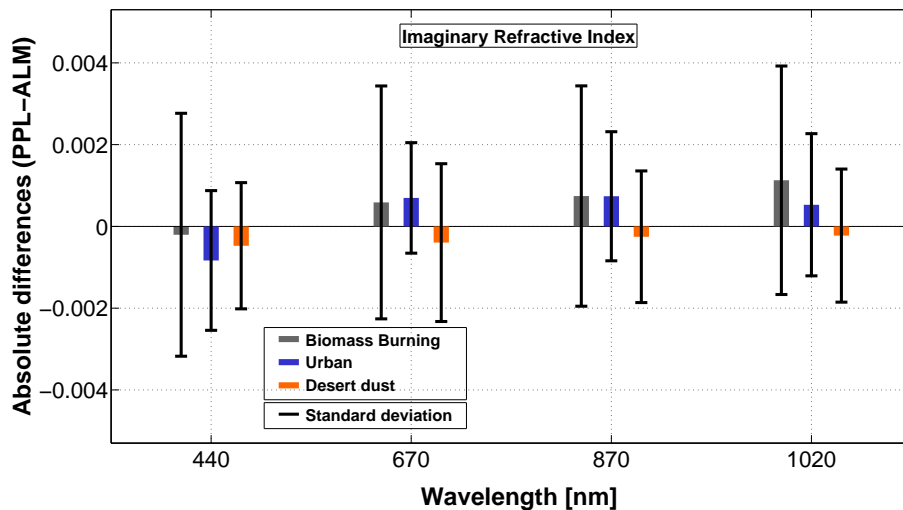


**Fig. 16.** Absolute differences (with sign) found in the imaginary part of the refractive index between the inversion obtained by almucantar and principal planes for the three analyzed cases (Table 4): biomass burning (gray bar) urban(blue bar) and desert dust (orange bar, only data from the first set (called Desert dust I)).

[Title Page](#)[Abstract](#)[Introduction](#)[Conclusions](#)[References](#)[Tables](#)[Figures](#)[|◀](#)[▶|](#)[◀](#)[▶](#)[Back](#)[Close](#)[Full Screen / Esc](#)[Printer-friendly Version](#)[Interactive Discussion](#)

## Sensitivity of aerosol retrieval to geometrical configuration

B. Torres et al.

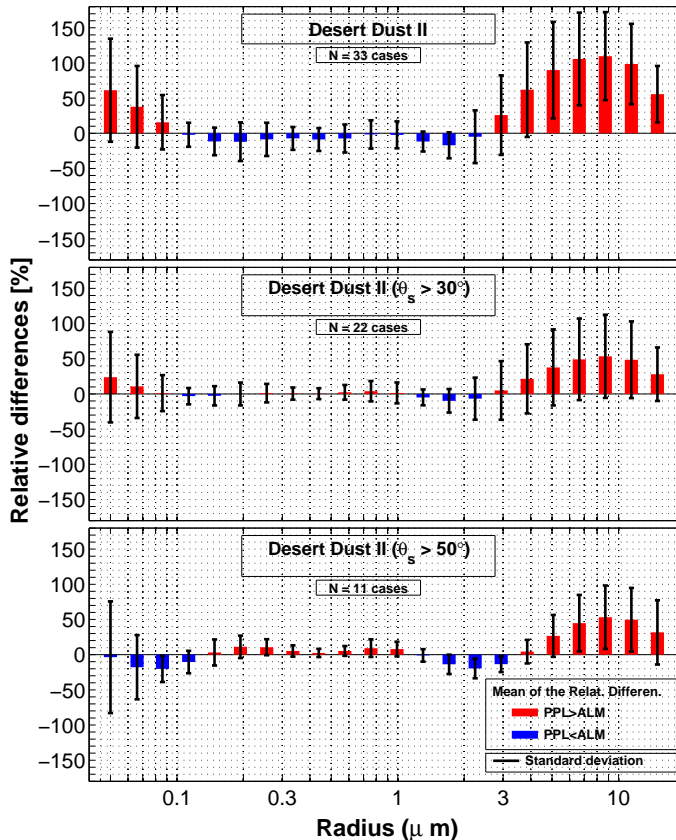


**Fig. 17.** Relative differences found in the size distribution between the inversion obtained by almucantar and principal planes for the photometers #233 and #33 in Solar Village site (data description in Table 4 case Desert dust II). The upper chart contains the comparison for the whole data set while the central and the bottom chart only for those data with the solar zenith angle larger than  $30^\circ$  and  $50^\circ$  respectively.